Standard Title Page - Report on Federally Funded Project

1. Report No. FHWA/VTRC 05-CR24	2. Government Accession No.	3. Recipient's Catalog No.	
4. Title and Subtitle Performance of a Bridge Deck with Glass Fiber Reinforced Polymer Bars as the Top Mat of Reinforcement		5. Report Date June 2005	
		6. Performing Organization Code	
7. Author(s) Kimberly A. Phillips, Matthew Harlan, Carin L. Roberts-Wollmann, Ph.D., P.E., and Thomas E. Cousins, Ph.D.		8. Performing Organization Report No. VTRC 05-CR24	
9. Performing Organization and Address Virginia Transportation Research Council 530 Edgemont Road Charlottesville, VA 22903		10. Work Unit No. (TRAIS)	
		11. Contract or Grant No. 64228	
12. Sponsoring Agencies' Name and Address Virginia Department of Transportation FHWA 1401 E. Broad Street P.O. Box 10249 Richmond, VA 23219 Richmond, VA 23240		13. Type of Report and Period Covered Final	
		14. Sponsoring Agency Code	
15. Supplementary Notes			

16. Abstract

The purpose of this research was to investigate the performance of glass fiber reinforced polymer (GFRP) bars as reinforcement for concrete decks. Today's rapid bridge deck deterioration is calling for a replacement for steel reinforcement. The advantages of GFRP such as its high tensile strength, light weight, and resistance to corrosion make it an attractive alternative to steel.

The deck of one end-span of the Gills Creek Bridge was constructed with GFRP bars as the top mat and epoxy-coated steel bars as the bottom mat. Live load tests were performed in 2003, shortly after completion of construction, and again in 2004. In addition, tests were performed on the deck of the opposite end-span, which had all epoxy-coated steel reinforcing.

The results of these tests were used to evaluate the girder distribution factors and impact factors of a GFRP reinforced bridge deck. In addition, a comparison of the results from the two test periods gives an indication of any changes in strains in the GFRP bars and if the deck is behaving differently than when first installed. The results were compared to the design standards specified by the American Concrete Institute in the *Guide for the Design and Construction of Concrete Reinforced with FRP Bar* to determine if the stresses in the deck were within the specified limits. The performances of the two end-spans were compared to determine if the GFRP reinforcement had any significant influence on overall bridge behavior.

There were no significant differences in the behavior of the deck after 1 year of service and there was no visible cracking. The behavior of the two end-spans was similar, and the measured girder distribution factors were less than the AASHTO design recommendations. The impact factors were less than design values for the 2003 tests but higher than design values for the 2004 tests. Stresses in the GFRP reinforcing bars were much less than the design allowable stress and did not change significantly after 1 year of service. The strain gauges, vibrating wire gauges, and thermocouples in the bridge deck were monitored for approximately 1 year using a permanent data acquisition system. Daily, monthly, and long-term fluctuations in temperature and stresses were examined. The vibrating wire gauges were more reliable than the electrical resistance strain gauges, and the main influence on strain changes was temperature fluctuation. A cost/benefit analysis of using GFRP bars indicates their high initial costs are justified when compared to the costs of a concrete overlay.

17 Key Words Glass fiber reinforced bars, composite materials, bridge decks, reinforced concrete		18. Distribution Statement No restrictions. This document is available to the public through NTIS, Springfield, VA 22161.	
19. Security Classif. (of this report) Unclassified	20. Security Classif. (of this page) Unclassified	21. No. of Pages 68	22. Price

Form DOT F 1700.7 (8-72)   Reproduction of completed page authorized

FINAL CONTRACT REPORT

PERFORMANCE OF A BRIDGE DECK WITH GLASS FIBER REINFORCED POLYMER BARS AS THE TOP MAT OF REINFORCEMENT

Kimberly A. Phillips
Graduate Research Engineer

Matthew Harlan
Graduate Research Engineer

Carin L. Roberts-Wollmann, Ph.D., P.E.
Assistant Professor

Thomas E. Cousins, Ph.D., P.E.
Associate Professor

Via Department of Civil and Environmental Engineering
Virginia Polytechnic Institute & State University

Project Manager
Michael C. Brown, Ph.D., P.E.

ABSTRACT

The purpose of this research was to investigate the performance of glass fiber reinforced polymer (GFRP) bars as reinforcement for concrete decks. Today's rapid bridge deck deterioration is calling for a replacement for steel reinforcement. The advantages of GFRP such as its high tensile strength, light weight, and resistance to corrosion make it an attractive alternative to steel.

The deck of one end-span of the Gills Creek Bridge was constructed with GFRP bars as the top mat and epoxy-coated steel bars as the bottom mat. Live load tests were performed in 2003, shortly after completion of construction, and again in 2004. In addition, tests were performed on the deck of the opposite end-span, which had all epoxy-coated steel reinforcing.

The results of these tests were used to evaluate the girder distribution factors and impact factors of a GFRP reinforced bridge deck. In addition, a comparison of the results from the two test periods gives an indication of any changes in strains in the GFRP bars and if the deck is behaving differently than when first installed. The results were compared to the design standards specified by the American Concrete Institute in the *Guide for the Design and Construction of Concrete Reinforced with FRP Bar* to determine if the stresses in the deck were within the specified limits. The performances of the two end-spans were compared to determine if the GFRP reinforcement had any significant influence on overall bridge behavior.

There were no significant differences in the behavior of the deck after 1 year of service and there was no visible cracking. The behavior of the two end-spans was similar, and the measured girder distribution factors were less than the AASHTO design recommendations. The impact factors were less than design values for the 2003 tests but higher than design values for the 2004 tests. Stresses in the GFRP reinforcing bars were much less than the design allowable stress and did not change significantly after 1 year of service.

The strain gauges, vibrating wire gauges, and thermocouples in the bridge deck were monitored for approximately 1 year using a permanent data acquisition system. Daily, monthly, and long-term fluctuations in temperature and stresses were examined. The vibrating wire gauges were more reliable than the electrical resistance strain gauges, and the main influence on strain changes was temperature fluctuation.

A cost/benefit analysis of using GFRP bars indicates their high initial costs are justified when compared to the costs of a concrete overlay.

FINAL CONTRACT REPORT

PERFORMANCE OF A BRIDGE DECK WITH GLASS FIBER REINFORCED POLYMER BARS AS THE TOP MAT OF REINFORCEMENT

Kimberly A. Phillips
Graduate Research Engineer

Matthew Harlan
Graduate Research Engineer

Carin L. Roberts-Wollmann, Ph.D., P.E.
Assistant Professor

Thomas E. Cousins, Ph.D., P.E.
Associate Professor

Via Department of Civil and Environmental Engineering
Virginia Polytechnic Institute & State University

INTRODUCTION

Bridge designers are faced with the challenge to remedy the increasing number of deteriorating bridge decks. According to Benmokrane et al. (2004), "[c]oncrete bridge decks deteriorate faster than any other bridge components because of direct exposure to the environment, deicing chemicals, and ever-increasing traffic loads." In the United States, $100 billion per year is wasted due to corrosion alone (Chong 1998).

One solution is the use of an increasingly popular material, fiber reinforced polymer (FRP) reinforcing bars. FRP bars are made of fibers pulled longitudinally that are held together by a resin. There are three commonly used types of fibers: glass (GFRP), carbon (CFRP), and aramid (AFRP). A new more experimental fiber material is basalt (BFRP). As a replacement for typical steel reinforcement, FRP has many advantages. It is a lighter material, so it is easier to transport and install in construction. FRP has a higher tensile strength than steel. It also is neutral to electrical and magnetic disturbances that may be caused by utilities and other elements on or near a bridge deck. Most importantly, FRP does not corrode like steel (Benmokrane et al. 2004). This makes FRP bars a promising alternative for the upper mat of reinforcement of bridge decks. Particularly in the northern states, salt and other chemicals that are used for deicing can permeate the deck and corrode the reinforcing bars. Even the freeze and thaw cycles can accelerate corrosion by causing water that gets into the cracks in the deck to freeze and expand, widening the crack and exposing the reinforcing bars to the environment.

To investigate the effectiveness and durability of GFRP bars as reinforcement for concrete decks, the Virginia Department of Transportation (VDOT) and the Virginia Transportation Research Council (VTRC) with funding provided through the Federal Highway

Administration's (FHWA) Innovative Bridge Research and Construction (IBRC) program worked with Virginia Tech to construct the Route 668 Bridge over Gills Creek in Franklin County, Virginia. The bridge was completed in July 2003 and is pictured in Figure 1. The deck of one span is reinforced with GFRP bars as the top mat and steel rebar as bottom mat. The other two spans are reinforced with steel bars as the top and bottom mat.

Figure 1. Route 668 Bridge Over Gills Creek

VDOT chose to use steel as the lower mat reinforcing due to some of the uncertainties of GFRP. VDOT wanted a proven material as the bottom mat. GFRP has a low modulus of elasticity, which could lead to excessive deflections and cracking. There is no conclusive research on the extent of deflection and cracking that would occur in an all GFRP-reinforced concrete deck. VDOT was especially concerned with the deck's long-term durability. Research has been done on durability, but only with accelerated lab testing which could have extreme results and may not be truly representative of the actual conditions in the field. The long-term durability of GFRP reinforced concrete decks is a serious issue that needs to be further explored to ensure the longevity of bridges.

During construction, the bridge was instrumented with devices to measure the temperature within the deck and the changes in strain of the GFRP bars. One of the all-steel reinforced spans was instrumented for comparison. The instrumentation of the bridge has been and continues to be used to perform short-term testing and long-term monitoring. Using the data collected, the changes in stress are evaluated and compared to design standards. Also, the long-term changes in stress can be used to identify significant changes in the deck condition or possibly reinforcing bar properties.

The basic mechanical properties of GFRP reinforcing bars are significantly different from conventional steel reinforcement. The modulus of elasticity is much lower, typically around 6000 ksi, compared to 29,000 ksi for steel. This lower modulus results in a much lower cracked stiffness for a GFRP reinforced section compared to a steel reinforced section with equal flexural strength. The lower modulus can also result in larger crack widths and lower shear strength for GFRP reinforced sections.

Another aspect of GFRP behavior that is quite different from steel reinforcing is that the stress-strain behavior is linear elastic until rupture. GFRP has no yield plateau, and therefore the philosophy used in steel reinforced concrete of allowing the steel to yield prior to concrete crushing is invalid. Instead the current design guidelines of ACI Committee 440 (2003) recommend that sections be designed to fail due to concrete crushing rather than GFRP bar rupture.

In the design of a bridge deck with GFRP reinforcing, the governing design factor tends to be limiting crack widths. When enough reinforcing is placed in the section to limit surface crack widths to 0.02 in, the calculated design flexural strength of the section is well above the factored moment demand. Even with the over-designed section, however, the cracked section moment of inertia is considerably smaller than the cracked moment of inertia of an equivalently designed steel reinforced deck, because of the relatively low modulus of elasticity of the GFRP bars. This more flexible cracked deck could influence global bridge behavior.

When designing a multi-girder bridge, according to the AASHTO LRFD Specifications (2004) a girder distribution factor (GDF) must be calculated to determine what fraction of a lane load is supported by a single girder. The GDF is a function of the type of deck, type of girder, number of loaded lanes, spacing of the girders, span length, depth of the concrete slab, and a longitudinal stiffness parameter. The GDFs for configurations with concrete decks were developed based on finite element analysis of bridges with typical steel reinforced concrete bridge decks (Zokaie et al., 1991).

Intuitively, it is understandable that if a deck were infinitely stiff the girders would share applied loads relatively equally, and if a deck were extremely flexible, the girders in close proximity to loads would carry the bulk of the loads. It is therefore conceivable that a GFRP reinforced deck, with a much lower cracked stiffness than a steel reinforced deck, might have significantly different girder distribution factors.

AASHTO allows a simplified strip method for the design of bridge decks. An equivalent strip width is determined based on the type of deck and the direction of the strip relative to the direction of traffic travel. Then the factored wheel load is divided by the strip width to determine a load per unit width on the slab. The slab is modeled as a continuous beam over rigid pinned supports, which represent the supporting girders. After the moment envelope is determined based on the worst case positioning of truck wheel loads, a critical location for positive and negative moment is determined, which is dependent on the girder type and flange width. The equivalent strip widths were also based on analysis of and experience with steel reinforced bridge decks. It is unknown if the reduced stiffness of the cracked section of a GFRP reinforced deck could influence the distribution of stresses within the deck caused by wheel loads.

Another aspect of GFRP material behavior that differs from steel is that it does not corrode. This characteristic makes GFRP bars very attractive in bridge decks to enhance their durability. Although GFRP bars do not produce corrosion byproducts that cause cracking and spalling of the concrete, such as those produced by steel corrosion, the GFRP bars do experience a loss of strength with time. This strength degradation must be quantified and accounted for in design.

Many researchers (Dejke 2001, Bhise 2002, Bank 1998, and Micelli et al. 2001) have studied the degradation of GFRP strength when it is exposed to alkalinity and moisture, such as the environment of GFRP bars embedded in concrete. Most studies have attempted to accelerate the rate of strength loss by placing the bars in completely saturated conditions at elevated temperatures. Several methods have been proposed to interpret the results of accelerated aging tests in order to predict retained strength of bars in typical bridge deck environments (Dejke 2001, Litherland et al. 1981, and Gentry et al. 2002)). However, as yet, there is no consensus on the correct approach.

The ACI 440 guidelines (2003) recommend the use of an environmental degradation factor to account for the strength loss with time. They recommend that for GFRP bars in concrete exposed to the environment, the retained strength at end of service should be assumed to be the 70% of the guaranteed tensile strength.

Based on this brief review, the areas of uncertainty in the design of bridge decks with GFRP reinforcement include the influence of the increased deck flexibility on girder distribution factors and equivalent strip widths for design, and the long-term behavior of the GFRP in a concrete environment exposed to weather.

PURPOSE AND SCOPE

The first objective of this research was to install instrumentation and perform live load testing on the Gills Creek Bridge. Live load tests were performed in the summer of 2003, shortly after completion of construction of the bridge and again in the summer of 2004. The initial live load test was performed shortly after the pouring of the deck. The follow-up live load testing was performed approximately 1 year after the initial testing. The results of the second tests are compared to the initial testing 1 year earlier.

The results of these tests were used to evaluate the girder distribution factors and impact factors of a GFRP reinforced bridge deck. In addition, a comparison of the results from the two test periods gives an indication of any changes in strains the GFRP bars may be experiencing and if the deck is behaving differently than when first installed. The results are compared to the design standards specified by the American Concrete Institute (ACI) in the *Guide for the Design and Construction of Concrete Reinforced with FRP Bars* to determine if the stresses in the deck are within the specified limits (2003).

The second objective of this research was to investigate the long-term behavior and durability of the GFRP reinforcing bars cast in a concrete deck. To accomplish this goal, the

bridge deck over Gills Creek was monitored for approximately 1 year using a permanent data acquisition system. The bridge deck has strain gauges, vibrating wire gauges, and thermocouples installed at specified locations within the slab. The topics of interest include daily, monthly, and long-term fluctuations in temperature and stresses in the bar and whether any change in behavior of the GFRP bars may be occurring.

METHODS AND MATERIALS

The Gills Creek Bridge was tested and monitored to investigate the long-term behavior and durability of GFRP reinforcing bars in concrete decks. The instrumentation and layout of the Gills Creek Bridge and the testing procedures are described in this section.

Route 668 Bridge Over Gills Creek

The bridge is a steel girder bridge composed of five W27x94 Grade 50 hot-rolled sections supporting each end span. Each girder is spaced center-to-center at 6 ft 6 in. The dimensions of the bridge deck over Gills Creek are shown in Figure 2. Span A is at the south end of the bridge. The two end spans are 45 ft in length with the center span measuring 80 ft in length for a total of 170 ft. The bridge's total width is 30 ft 4 in.
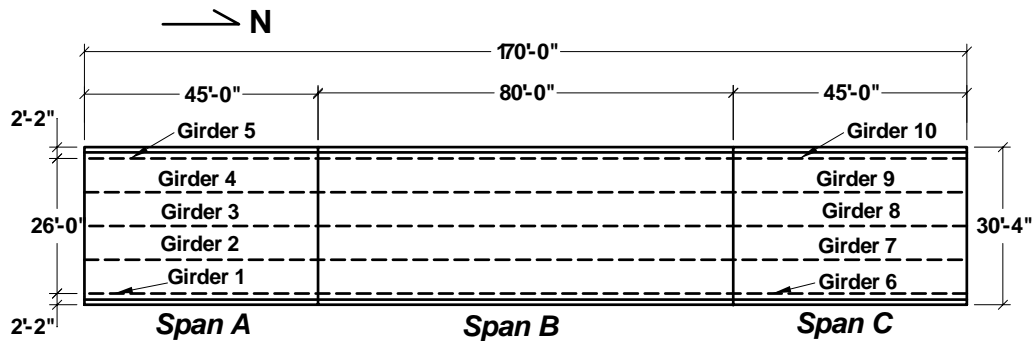

Figure 2. Plan View of Gills Creek Road

Construction Observations

The construction of the bridge was monitored closely by the research team, starting from the initial observation of the previous structure to the opening of the new bridge to traffic. The most important process to be observed was the bridge deck construction, or more specifically, the installation of both the epoxy-coated steel bars and the GFRP bars. The total man-hours required to install the reinforcement in both Span A and Span C was noted. Additionally, comments and complaints from the construction crew were logged. Handling of the bars and familiarity with the material, or lack thereof, were important considerations to be recorded. The in-place appearance and the flexibility of the steel and GFRP mats of reinforcement were noted. Finally, the observations were compared to develop conclusions on the constructability of decks reinforced with GFRP.

Bridge Deck Instrumentation and Layout

The bridge deck is reinforced concrete with a minimum thickness of 8 in between the girders and 9 in at the overhangs. Spans B and C have a top and bottom mat of epoxy-coated steel reinforcing bars. The longitudinal bars are No. 4 steel bars, and the transverse bars are No. 6 steel bars. Span A has a top mat of GFRP bars and a bottom mat of steel bars. The bottom mat of Span A is the same as the other two spans with No. 4 and No. 6 steel bars. The top mat is comprised of all No. 6 GFRP bars. The design minimum concrete cover to the center of the bar is 2¾ in for the steel bars and 2 in for the GFRP bars. Figure 3 presents a partial cross-section of Span A.
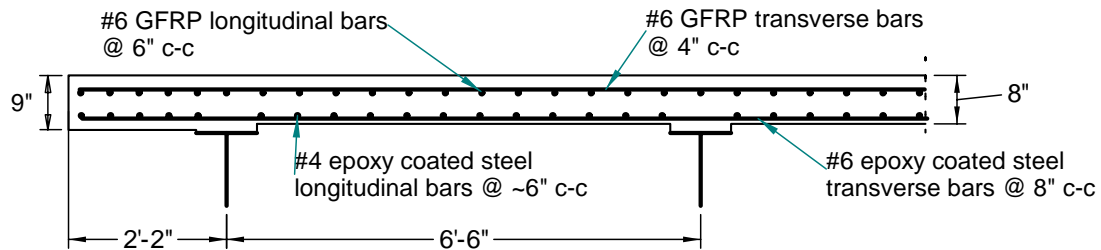

Figure 3. Partial Cross-section of Span A

Span A

Figure 4 presents the Span A instrumentation layout. Span A was instrumented with electrical resistance (ER) strain gauges, vibrating wire (VW) gauges, and thermocouples. The lead wires of all the gauges and the thermocouple wires run through an access hole in the metal deck form and through a PVC pipe for easy accessibility for testing. All of the gauges and thermocouples were monitored with a permanent datalogger, and the ER strain gauges were used for the live load testing.

Electrical Resistance Strain Gauges

Span A was instrumented with four sets of ER strain gauges. All of the gauges were applied to the top mat of GFRP reinforcement. The first group was located near the south abutment above the first interior girder. Four transverse bars were gauged with two gauges, one at each side of the top flange of the steel girder, for a group total of eight ER strain gauges. These eight gauges were labeled ATA1 through ATA8 representing the location of Span 'A' on the 'T'ransverse bars at the 'A'butment.
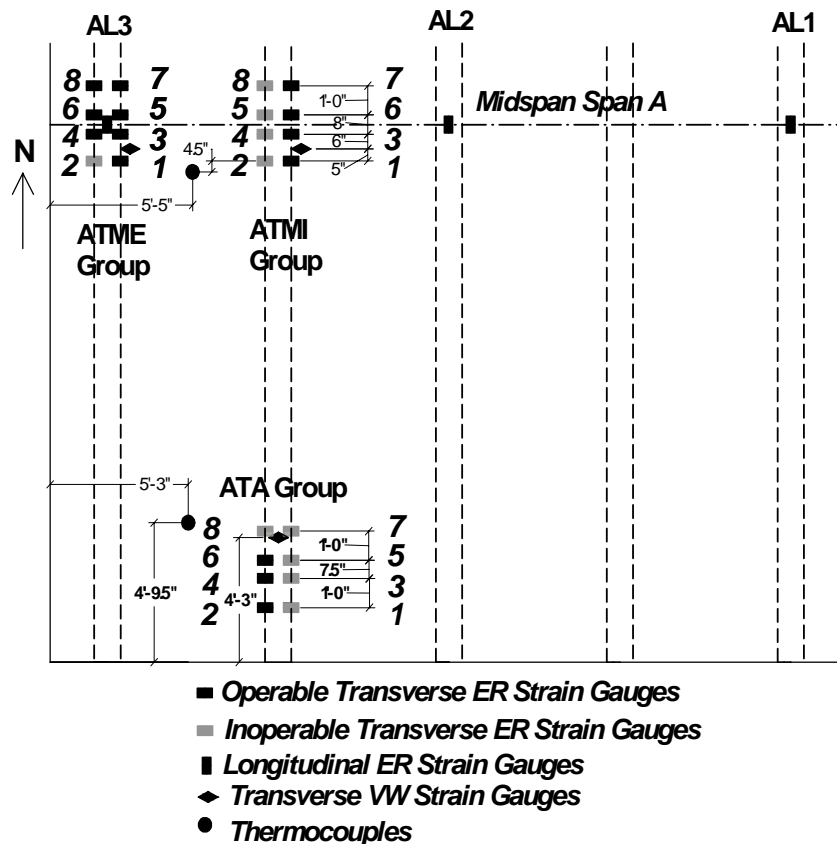
Figure 4. Span A Instrumentation Plan with Status for 2004 Tests

The second group was located at the midspan of Span A above the first interior girder. Similar to the first group, four transverse bars were gauged with one gauge at each side of the top flange of the girder, totaling to eight ER strain gauges. These gauges were labeled ATMI1 through ATMI8 representing the location of Span 'A' on the 'T'ransverse bars at the 'M'idspan 'I'nterior girder.

The third group was located over the exterior girder at midspan. The same bars as the second group were gauged at the edges of the exterior girder's top flanges. These gauges were labeled ATME1 through ATME8 representing the location of Span 'A' on the 'T'ransverse bars at the 'M'idspan 'E'xterior girder.

The fourth set was applied to the upper mat longitudinal bars of Span A at midspan. There were three gauges, one located above each exterior girder and one located above the center girder. These gauges were labeled AL1 through AL3 representing the location of Span 'A' on the 'L'ongitudinal bars.

All ER strain gauges were installed using procedures recommended by the manufacturer. Prior to weatherproofing, insulated lead wires were soldered to the gauges and run through the deck to a common access point located close to the abutment. The gauges were then weatherproofed using materials and procedures recommended by the manufacturer. Typically, lead wires were bound to the bottom mat reinforcement to protect them from worker's boots and

from jostling during placing of concrete. An access hole was drilled in the stay-in-place metal deck forms and a small section of PVC pipe was installed in the hole with caulking between the PVC and the deck forms. The lead wires were then fed through the pipe, and the remaining open space in the pipe was filled with duct tape. Great care was taken to ensure that each wire was labeled properly and also that the wires were sufficiently long to reach the mobile data acquisition system.

Vibrating Wire Strain Gauges

Vibrating wire (VW) strain gauges were also installed in the bridge deck. VW gauges are more accurate and last longer than ER strain gauges, however they are also more expensive. Due to the higher expense, only two VW gauges were placed at three critical locations: the first interior girder at the abutment, the first interior girder at the midspan, and the first exterior girder at the midspan of the bridge.

At each location a gauge was installed at the top mat and the bottom mat. The strains measured by the top mat VW strain gauges are compared to the strains measured by the ER strain gauges in the Results section. The strains measured by the bottom mat VW strain gauges are used to determine the location of the neutral axis of the deck to see if the deck is cracked. The VW gauge at the abutment on the top mat is labeled VAT representing the 'V'ibrating wire gauge located at the "A'butment on the 'T'op mat. Similarly, the gauge at the abutment on the bottom mat is labeled VAB. The gauges at the midspan over the interior girder are labeled VMIT and VMIB, and the gauges at the midspan over the exterior girder are labeled VMET and VMEB with the 'T' and the 'B' indicating the top and bottom mat, respectively.

All VW strain gauges were installed and connected to lead wires using procedures recommended by the manufacturer. Unlike the ER strain gauges, the VW strain gauges did not have to be weatherproofed. The lead wires were fed through the deck and the access hole similarly to the ER strain gauges. Each lead wire was labeled carefully.

Thermocouples

Thermocouples are located over the interior girder at the abutment and at midspan. At each location there is a thermocouple located at the top mat of reinforcement, the bottom mat of reinforcement, and in between the two mats. The thermocouples are used to monitor the temperatures within the bridge deck. The thermocouples are labeled TAT, TAM, TAB, TMT, TMM, and TMB. Each label indicates the instrumentation type ('T'hermocouple), location over the interior girder ('A'butment or 'M'idspan), and the location within the deck ('T'op, 'M'iddle, or 'B'ottom).

Span C

Span C was instrumented with only ER strain gauges. The layout of the instrumentation can be seen in Figure 5. Just like Span A, the lead wires of the gauges are easily accessible through an access hole in the metal deck form. The strain gauges were used for live load testing. Span C was not monitored by a permanent datalogger.
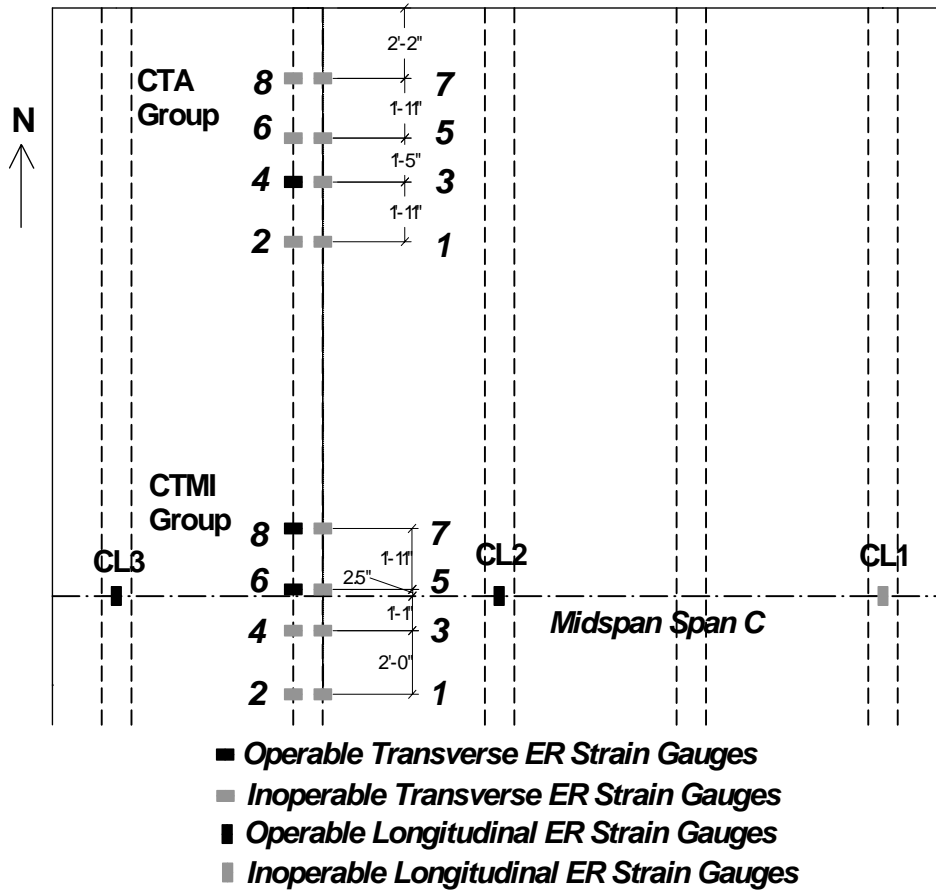
Figure 5. Span C Instrumentation Plan with Status from the 2004 Tests

Electrical Resistance Strain Gauges

Span C was instrumented with three sets of ER strain gauges. All of the gauges were applied to the top mat of steel reinforcement. The first group was located near the north abutment above the first interior girder. Four transverse bars were gauged with one gauge at each side of the top flange of the steel girder, for a group total of eight ER strain gauges. These eight gauges were labeled CTA1 through CTA8 representing the location of Span 'C' on the 'T'ransverse bars at the 'A'butment.

The second group was located at the midspan of Span C above the first interior girder. Similar to the first group, four transverse bars were gauged with one gauge at each side of the top flange of the girder, totaling to eight ER strain gauges. These gauges were labeled CTM1 through CTM8 representing the location of Span 'C' on the 'T'ransverse bars at 'M'idspan.

The third set was applied to the upper mat longitudinal bars of Span C at midspan. There were three gauges, one located above each exterior girder and one located above the center girder. These gauges were labeled CL1 through CL3 representing the location of Span 'C' on the 'L'ongitudinal bars.

Bridge Deck Casting

After the reinforcing bars were installed and the embedded gauges were secured in the deck, concrete was placed into the forms. The casting was accomplished in one day, with all three simple spans cast in one operation. The contractor started at the abutment side of Span C and continued across the bridge, finishing at the abutment side of Span A. Figure 6 shows the casting operation at the beginning of the day in Span C. Test cylinders of concrete placed in Spans A and C were made during the casting operation. The cylinders were then match-cured with the deck for approximately two weeks and then taken back to Virginia Tech for storage. When tested for 28-day compressive strength, the Span A cylinders averaged 7001 psi and the Span C cylinders averaged 6882 psi.

Figure 6. Span C Concrete Casting

Great care was taken by the researcher as well as the construction workers to avoid contact with the installed gauges and wires during the casting operation. However, it should be noted that concrete was placed with a bucket about one to two feet above the bars, and in some cases this concrete was dropped directly on top of a section where gauges and thermocouples were present. Also, it should be noted that the workers tried to stay clear of the gauged sections while walking on the top mat of reinforcement. However, this was not always the case. Figure 7 shows the casting operation in the Span A end of the bridge.

Test Preparation Procedures

A truck-mounted under-bridge inspection platform, or Moog, was used to provide easy access to the underside of the superstructure. VDOT provided the inspection platform and the testing truck. For the 2003 tests, the bridge had not yet been opened to traffic, so construction

detours were still in place. For the 2004 tests, traffic control for the two days of setting up and live load testing was provided by VDOT.

Figure 7. Span A Concrete Casting

Bridge Girder Instrumentation

Electrical Resistance Gauges

For the 2003 tests, three beams in Span A and Span C (the two exterior beams and the center beam) had strain gauges applied on the top and bottom flanges. The intent was to investigate the strain profile through the depth of the composite cross-section. For the 2004 tests, each steel girder of Span A and C had new strain gauges applied to the top of the bottom flange at midspan. An ER gauge is pictured in Figure 8. The strains recorded by the strain gauges were used to calculate the girder distribution factors and the dynamic load allowances. ER strain gauges were not applied on the top flange as in the 2003 test because the data collected from the top flanges did not provide very useful information.

Deflectometers

For the 2003 and 2004 tests, deflectometers were clamped to the bottom flange of each girder at the midspan of Spans A and C. A deflectometer is pictured in Figure 9. They are made of an aluminum plate between two thicker aluminum plates. The cantilevered plate in the middle is gauged with four strain gauges that are weatherproofed. At the end of the cantilevered plate is a metal loop. The metal loop was attached to a weight at ground level with wire, to pre-deflect the deflectometer approximately 1 in before the testing. The pre-deflection caused a strain in the top of the plate. When the truck ran over the bridge causing the girders to deflect, the decrease in strain was measured and converted to a corresponding deflection. During each test, the

deflection of the girder was recorded. The deflectometers were calibrated in the laboratory prior to each test.

Figure 8. ER Strain Gauge on Steel Girder

Figure 9. Deflectometer Clamped to Steel Girder

Weigh-In-Motion Gauges

In 2004, weigh-in-motion (WIM) gauges were also clamped to each steel girder at the midspan of Spans A and C, except girder 6. Figure 2 shows the numbering system of the girders. Girder 6 was not instrumented because only nine WIM gauges were available for use. The WIM gauges

were also used to calculate the girder distribution factors and dynamic load allowance for Spans A and C. The results were compared to those of the deflectometers and the ER strain gauges to see if the WIM gauges had similar results. WIM gauges are easier to install than ER strain gauges, so it would be optimal to be able to use only WIM gauges in future testing. The WIM gauges were clamped to the underside of the bottom flange of each girder. Each gauge had a short cable already attached to it. Longer cables were used to connect the short cables to the mobile data acquisition system. The WIM gauges were supplied by VTRC.

Data Acquisition

The bridge girder instrumentation and the ER strain gauges located in the bridge deck were connected to a mobile data acquisition system for the live load testing. The system was the Megadac 3108 AC data acquisition system from Optim Electronics.

Live Load Testing

The first live load tests on the Gills Creek Bridge were performed on June 23, 2003 and the second live load tests were performed on June 17, 2004, approximately 1 year after the initial live load testing was performed.

Truck Description

The same dump truck from VDOT was used for the live load testing of the bridge deck in 2003 and in 2004. The truck was loaded with stone at a quarry. The front axle of the truck weighed 16.1 kips and the rear axle weighed 33.6 kips in 2003. In 2004 the front axle weighed 13.5 kips and the rear axle weighed 36.3 kips. The rear axle consisted of two axles, so the weight was assumed to be split between the two. The front wheels measured 6 ft-9 in center-to-center and 7 ft-10 in out-to-out. The rear wheels measured 6 ft center-to-center and 8 ft-4 in out-to-out. The distance between the first and second axle was 14 ft 10 in and between the second and third axle was 4 ft 5 in. The dump truck is pictured in Figure 10.

Truck Orientations

All testing was performed in the southbound lane of traffic on the bridge. There were two truck orientations. One was with the truck's front left wheel over the exterior girder. A line was marked one foot from the face of the parapet (25.5 in from the edge of the deck) to indicate the center of the exterior girder. This orientation was chosen in the initial live load test to load the overhang as much as possible. The truck was positioned as close as it could safely get to the edge. Although this orientation did not result in the greatest effect on the overhang, it did create the greatest effect on the exterior girder.

The second orientation was with the truck straddling the first interior girder. A line was marked 4 ft from the face of the parapet to indicate the location of the front wheel of the truck. This position created the greatest effect on the first interior girder.

Figure 10 VDOT Dump Truck Used for Live Load Testing

Quasi-Static and Dynamic Tests

The quasi-static test had the truck moving just fast enough to prevent any jerky or unsteady movements. This test represented a static loading on the bridge. A test was characterized by the VDOT truck crossing the span of interest as the strains and deflections were recorded by the mobile data acquisition system. After crossing the span, the truck would stop and cross back over the span in reverse to get the readings for the next test.

For the dynamic test, the truck started about 300 ft away from the bridge and built up a speed of approximately 50 mph when it crossed the bridge. This was the fastest safe speed at which the overloaded truck could travel. After crossing the bridge, the truck turned around and crossed the bridge going the opposite direction.

The following information was recorded for each test:
- Data set number
- Direction that the truck was traveling (northbound or southbound)
- The orientation of the truck (exterior or interior)
- The speed of the truck (assumed to be zero for the quasi-static testing)

Table 1 presents the number and types of tests performed in Span A and Span C in 2003 and 2004.

Table 1. Test Matrix

	2003 Tests			2004 Tests		
	Interior Quasi -static	Interior Dynamic	Exterior Quasi -static	Interior Quasi -static	Interior Dynamic	Exterior Quasi -static
Truck Crossings in Span A	5	6	5	5	6	5
Truck Crossings in Span C	5	6	5	5	6	5

Long-term Data Acquisition

To collect the long-term data, a CR23X Micrologger made by Campbell Scientific, Inc. was used. This device runs off of a user-provided program that specifies which channels are being used and at what frequency the readings are to be taken. The programs and the wiring diagram for the Campbell installed at the bridge are presented in Phillips (2004). Readings were taken every hour for approximately 1 year.

The Campbell was used to monitor the instrumentation of Span A of the Gills Creek Bridge. Since there were not enough ports to connect all of the instrumentation on the datalogger itself, additional boards had to be used. Two multiplexers were used, one for the ER strain gauges and one of the VW gauges. The thermocouples were connected directly to the Campbell. All of the components were screwed to a plate that was then secured in an environmentally resistant box. Figure 11 is a picture of the datalogger. After programming the datalogger in the lab, it was taken to the field location and the lead wires of the instrumentation were run through the access hole in the box and connected to the datalogger. Weatherproofing putty provided by the box manufacturer was placed in the access hole to fully seal the box, and desecant packs were placed in the box to control the internal humidity. The box was locked and placed on the south abutment wall on the underside of the bridge. A solar panel was mounted on the parapet of the bridge to ensure that the datalogger had a constant power source.
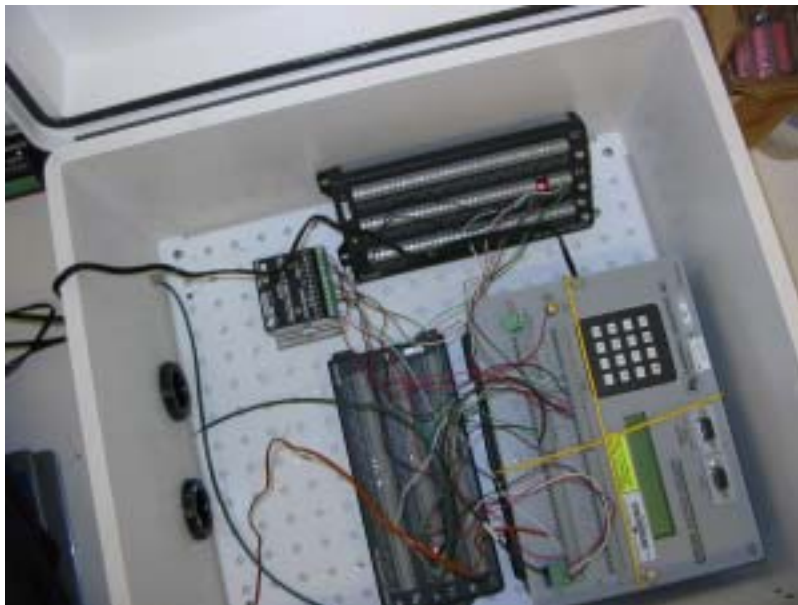

Figure 11. CR23X Micrologger and Instrumentation Components

The data acquisition system was installed on November 20, 2004. Each strain gauge was tested with a voltmeter to make sure that it had the correct resistance of 350 ohms across it, indicating whether it was still working properly. The working strain gauges were then connected to the Campbell. Figure 4 indicates which strain gauges were operable at the time of installation. The vibrating wire gauges and thermocouples were connected as well. The readings were monitored for approximately 1 year.

RESULTS

Live Load Tests

Live load tests were performed on the bridge on June 23, 2003, and on June 17, 2004, approximately 1 year after the initial testing. The data was collected at a rate of 400 readings per second. This was a large number of data points to analyze, especially for the quasi-static tests that lasted for around thirty seconds. For all the quasi-static tests, a program was applied to keep only one out of every 10 data points. For all the tests on Span A, both quasi-static and dynamic, a three-point running average was applied to the remaining points. The dynamic tests on Span C were not reduced or averaged. All of the analyses of the live load tests were performed using the final data. This section investigates the behavior of the bridge during testing and compares the bridge's performance in 2003 to the performance in 2004.

Transverse Deck Strains

During the live load testing of the Gills Creek Bridge, the strains in the GFRP bars were recorded using the ER strain gauges in the bridge deck. As stated previously, there were four sets of gauges in Span A with three of those sets used for measuring transverse strains. The locations of the three sets were at the abutment over the interior girder, at the midspan over the exterior girder, and at the midspan over the interior girder. All of the gauges from the initial live load test were still working. There were enough gauges in each section to determine a transverse stress profile for each location. However, Span C only had five gauges working, so the strains could not be used to determine a profile. Figure 4 and Figure 5 show the operable gauges.

To find the transverse stress profile at each location in Span A, several steps were taken. With each truck crossing, the strain in each gauge was recorded. Each group of gauges was analyzed separately. For each gauge, the maximum strain was determined along with the time that the maximum strain occurred. The time when the highest maximum strain in the group occurred was identified. The strains that were measured at that time were recorded for all the gauges in the group. These strains were converted to stresses using the modulus of elasticity determined from testing of the GFRP bars, 5,900 ksi (Harlan (2004)). A stress profile was plotted for each group using the stresses at the time of maximum strain. Essentially, it is like taking a snapshot in time and recording the stresses in each bar at that moment. This process was performed for each of the three groups of ER strain gauges. Examples of the calculations performed to determine the stresses are presented in Harlan (2004) and Phillips (2004).

The stresses calculated for each bar were plotted against the gauge location to generate a transverse stress profile for the three gauging locations. For comparison, the allowable tensile stress was calculated. A sample of the GFRP bars was tested in the laboratory and the average ultimate tensile strength was found to be 109 ksi with a standard deviation of 3.23 ksi (Harlan (2004)). According to the *ACI Guide for Design and Construction of Concrete Reinforced with FRP Bars* reported by ACI Committee 440 (2003), the design tensile strength should be calculated using the following equation:

$$f_{fu} = C_E f^*_{fu}$$

(1)

where f_{fu} is the design strength of FRP taking into consideration reductions for the service environment, C_E is the environmental reduction factor which for GFRP in concrete exposed to earth and weather is 0.7 or 70%, and f^*_{fu} is the guaranteed tensile strength of an FRP bar. The guaranteed tensile strength is found by taking the average tensile strength of samples, $f_{u,ave}$, minus three times the standard deviation, σ. Applying this equation, $f^*_{fu} = 109-3(3.23) = 99.3$ ksi. Then plugging the results into Equation (1), $f_{fu} = 0.7(99.3) = 69.5$ ksi. ACI 440 specifies in Table 8.2 that for GFRP the creep rupture stress limit is equal to $0.20f_{fu}$. Applying this equation, the allowable tensile stress for the GFRP bars is 0.2(69.5) or 13.9 ksi. ACI 440 does not specify an allowable compressive stress for FRP.

The allowable stress for the GFRP can also be calculated using the guaranteed tensile strength used in design which is not as high as the actual strength measured in the lab. The GFRP bars in the deck are Grade F70, which corresponds to a guaranteed tensile strength of 70 ksi. Applying Equation 1 to an f^*_{fu} value of 70 ksi, $f_{fu} = 0.7(70) = 49$ ksi. That would make the design allowable tensile stress 0.2(49) or 9.8 ksi.

Figure 12 shows the stresses based on the measured strains in the strain gauges on the GFRP reinforcement in the group of gages near the abutment (ATA gauges) for the Interior Truck configuration. The stresses are the averages for all similar truck crossings. The figure shows stresses from both the static and dynamic tests in 2003 and 2004. The first observation from the graph is that the stresses are primarily tensile, but are very small, less than 100 psi. It can also be seen that the stresses from the dynamic tests are higher (more tensile) than the static tests. Also note that the stresses are relatively uniform across the instrumented region.
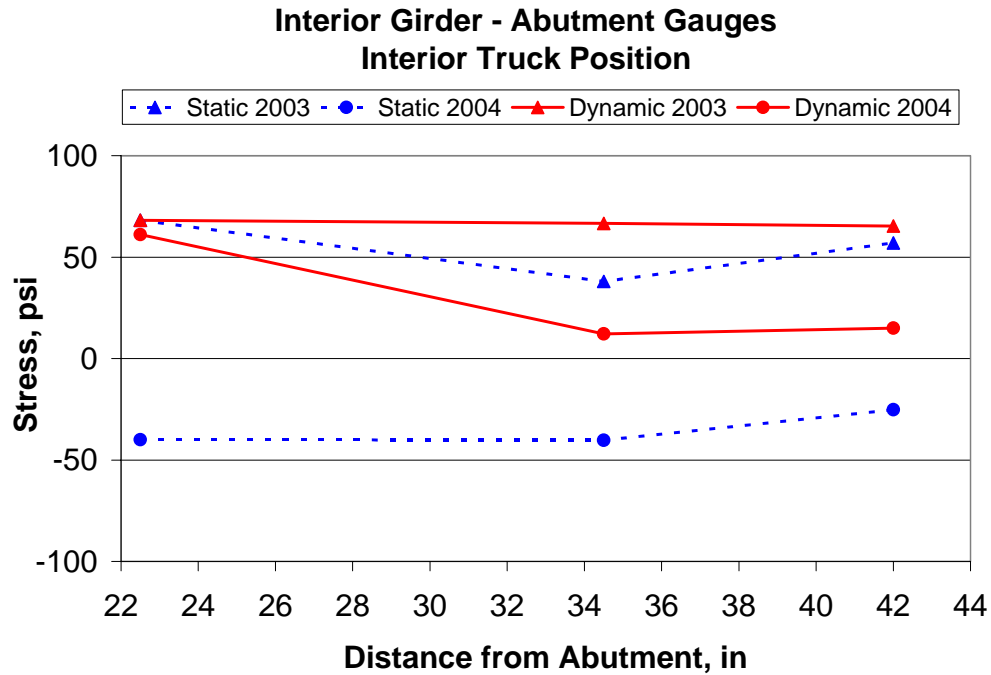
Interior Girder - Abutment Gauges
Interior Truck Position

Figure 12. Stresses in GFRP Bars at Interior Girder Near Abutment from Interior Truck Crossing

Figure 13 presents the stresses based on the measured strains in the strain gauges on the GFRP reinforcement in the group of gauges near midspan over the interior girder (ATMI gauges) for the Interior Truck configuration. The figure shows average stresses from both the static and dynamic tests in 2003 and 2004. It can be seen from the graph that the stresses are primarily compressive, and are also very small, less than 150 psi. The compressive stresses are due to the fact that the bridge deck is bending transversely due to the truck load. Although the model used to design bridge decks assumes that the deck is continuous over rigid supports, in reality the supports (the beams) are flexible. Since the beams directly under the load deflect more than the more distant beams, the overall deflected shape of the deck in concave upwards. This means that the entire top mat of reinforcement can be expected to be in compression, as was measured. It can also be seen that the stresses from the dynamic tests are more compressive than the static tests. And, as with the abutment gauges, the measured stresses are relatively uniform across the instrumented region.
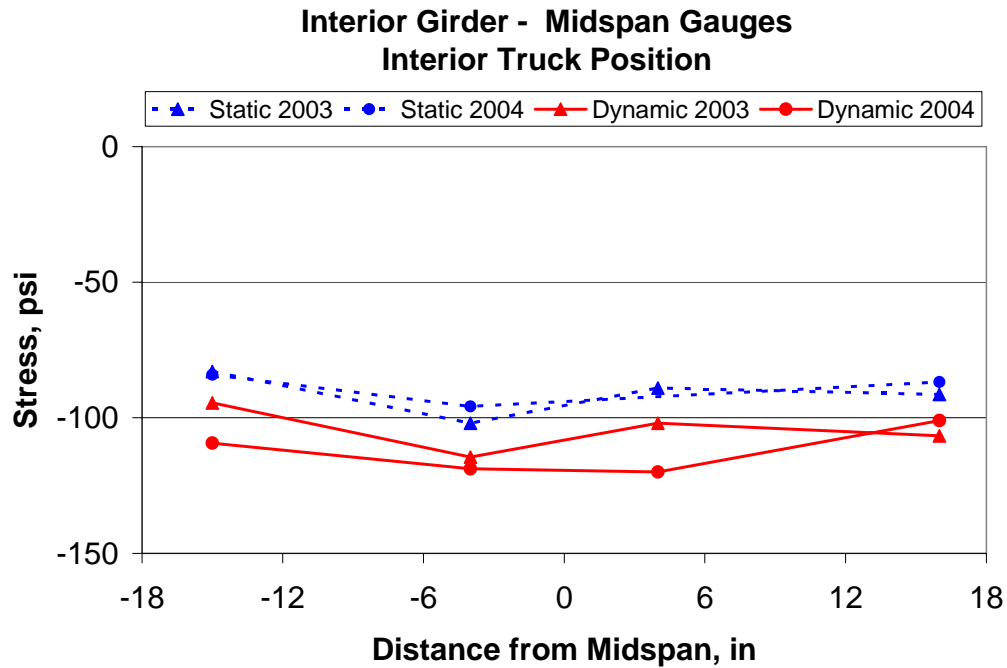
Interior Girder - Midspan Gauges
Interior Truck Position

Figure 13. Stresses in GFRP Bars at Interior Girder Near Midspan from Interior Truck Crossing

Figure 14 presents the stresses based on the measured strains in the strain gauges on the GFRP reinforcement in the group of gauges near midspan over the exterior girder (ATME gauges) for the Interior Truck configuration. The figure shows stresses from both the static and dynamic tests in 2003 and 2004. The stresses in these bars are extremely small, showing slight tension in the 2003 tests and slight compression in the 2004 tests. There are only slight differences between the static and dynamic tests. Since this is the exterior girder, and there is no applied load on the overhang, the model used to design the deck would predict no strain in these gages due to the interior truck configuration.
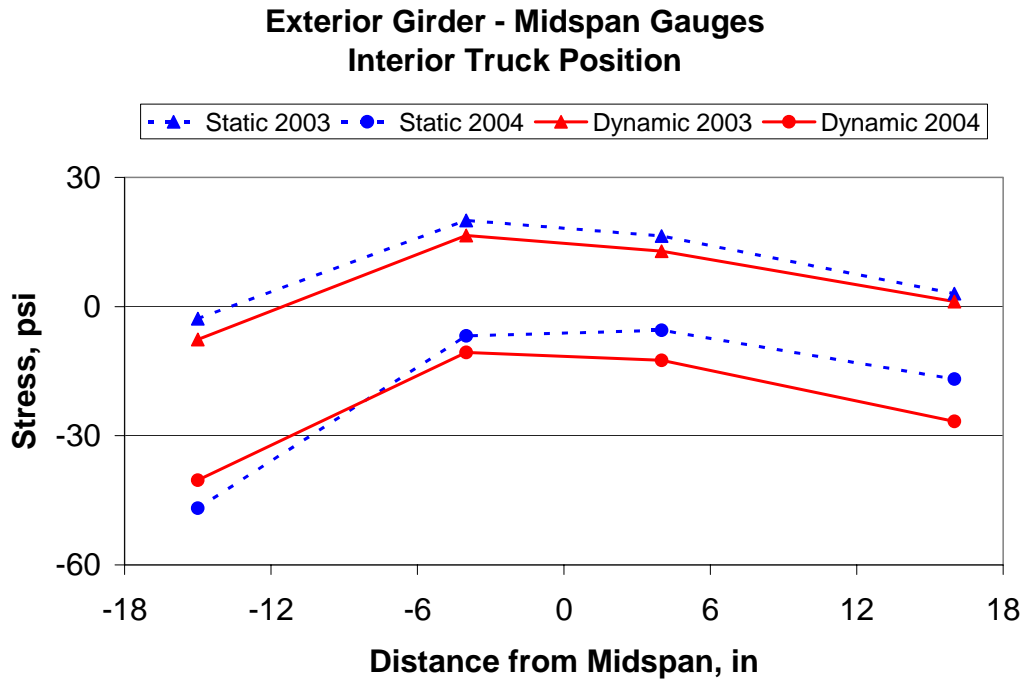
Exterior Girder - Midspan Gauges
Interior Truck Position

Figure 14. Stresses in GFRP Bars at Exterior Girder Near Midspan from Interior Truck Crossing

Figure 15 presents the stresses based on the measured strains in the strain gauges on the GFRP reinforcement in the two groups of gauges near midspan over the interior and exterior girders (ATMI and ATME gauges) for the Exterior Truck configuration. The figure shows stresses from the static tests in 2003 and 2004. There were no dynamic tests performed for this truck configuration. As for the interior truck configuration, the stresses in the GFRP bars over the interior girder are compressive and less than 150 psi in magnitude. The stresses in the bars over the exterior girder are quite small, and were more tensile in the 2003 tests. It can be seen that there are only very small changes in the measured stresses from 2003 to 2004. It can also be seen that the stresses are relatively uniform over the instrumented region.

Figure 16 presents the stresses based on the measured strains in the strain gauges on the GFRP reinforcement in the group of gauges near the abutment over the interior girder (ATA gauges) for the Exterior Truck configuration. The figure shows stresses from the static tests in 2003 and 2004. As mentioned above, there were no dynamic tests performed for this truck configuration. The stresses in 2003 were primarily tensile, but were quite small, and uniform over the instrumented region. In 2004 the stresses were primarily compressive, and were less uniform over the region. It is unclear if this is true behavior or due to a malfunctioning strain gauge. In any case, all measured stresses from truck crossings were quite small, less than 120 psi.

The overall observations that can be made from these measurements are that the stresses in the bars are very small, due to the fact that the deck is uncracked, the stresses at midspan are primarily compressive, there are only slight changes in measured stresses from 2003 to 2004, and the stresses are quite uniform over the instrumented regions, indicating a large width of the deck participating in carrying the wheel loads to the girders.

Interior and Exterior Girders - Midspan Gauges
Exterior Truck Position
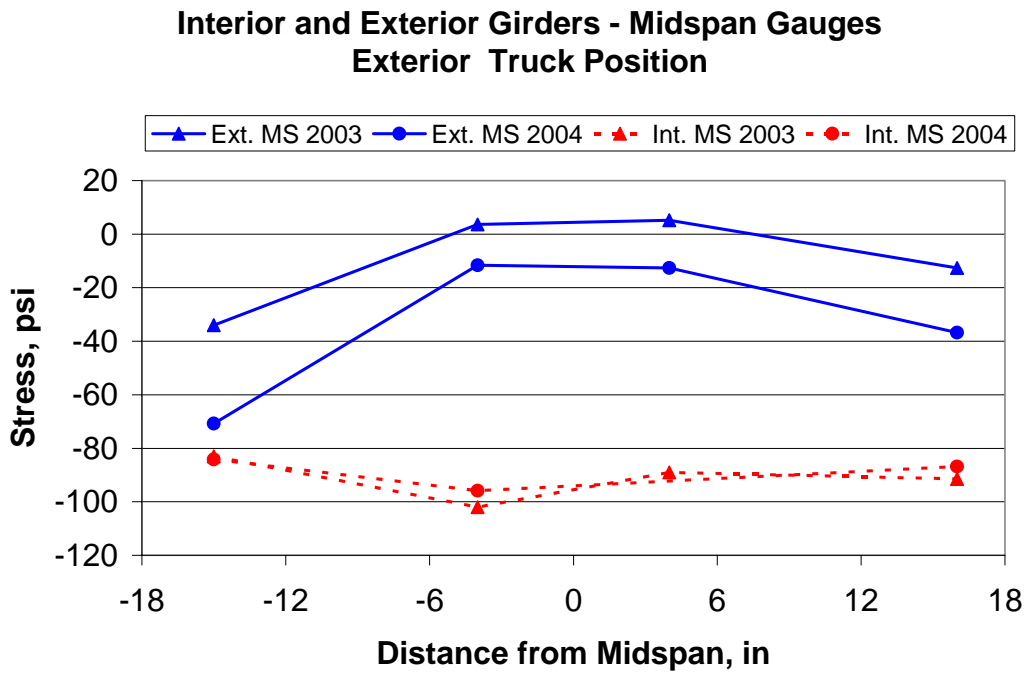
Figure 15. Stresses in GFRP Bars Near Midspan from Exterior Truck Crossing

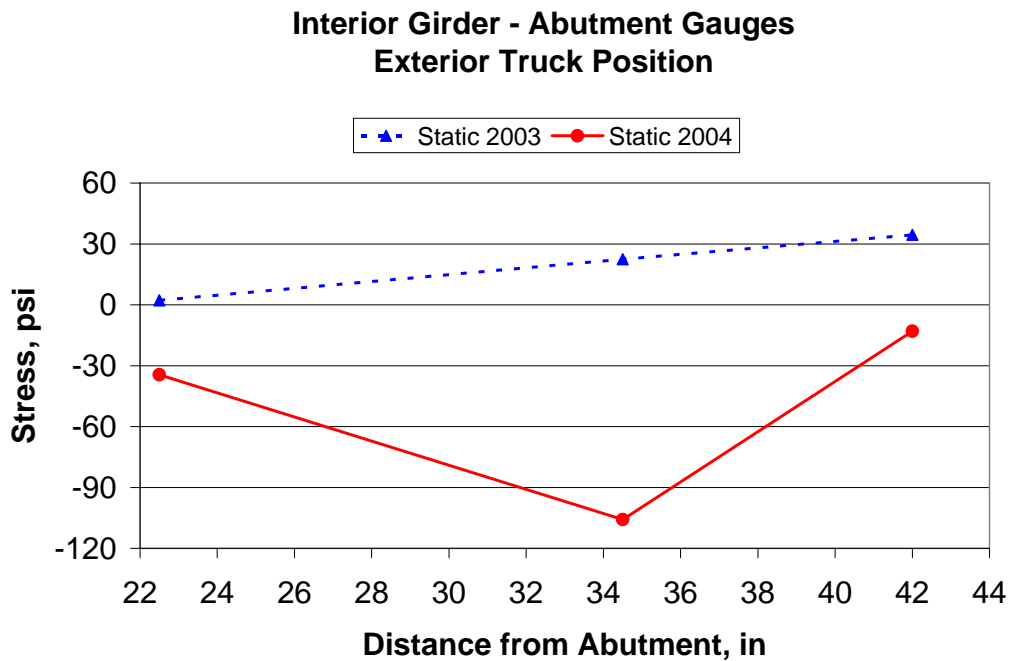**Interior Girder - Abutment Gauges**
Exterior Truck Position

Figure 16. Stresses in GFRP Bars Near Abutment from Exterior Truck Crossing

Girder Distribution Factors

Introduction and AASHTO Equations

The girder distribution factor (GDF) is used in design to determine what fraction of the total load is being carried by a single girder. The GDF is then applied to the design loads when designing the bridge. Two documents produced by the American Association of State Highway and Transportation Officials (AASHTO) outline how to determine the required GDF.

The AASHTO Standard Specification (2002) defines the GDF to be used dependent on the bridge's type of superstructure. The GDF for a wheel load for an interior girder is defined with the following equation:

$$g = S\!\!\Big/\!\!D \qquad\qquad (2)$$

where g = GDF for a wheel line
S = center-to-center spacing of the interior girders
D = denominator dependent on type of deck and girders

Table 3.23.1 of the AASHTO Standard Specification tabulates the GDF values to be used. For a concrete bridge deck with steel I-beam stringers, the distribution factor is S/7.0 for bridges designed for one traffic lane and S/5.5 for bridges designed for two traffic lanes. For the exterior girder distribution factors, the AASHTO Standard Specification states to use the assumption that the deck acts as simple spans between the girders to determine the bending moment reaction at the girder from the live load. This process is known as the lever rule.

The AASHTO LRFD Specifications (1998) provides equations in Table 4.5.2.2.2b-1 to calculate the distribution of live loads per lane for moment in interior beams. For a concrete bridge deck on steel beams with one design lane loaded, the following equation applies:

$$g = 0.06 + \left(\frac{S}{14}\right)^{0.4}\left(\frac{S}{L}\right)^{0.3}\left(\frac{K_g}{12.0Lt_s^3}\right)^{0.1} \qquad\qquad (3)$$

where g = GDF for interior beams (fraction of truck or lane load)
S = center-to-center spacing of interior girders (ft)
L = span length (ft)
t_s = thickness of deck slab (in)
K_g = longitudinal stiffness parameter.

K_g is defined in Equation 4.6.2.2.1-1 of the AASHTO LRFD Specifications, which is the following:

$$K_g = n\left(I + Ae_g^2\right) \qquad\qquad (4)$$

where n = modulus of elasticity of beam material (ksi) divided by the modulus of elasticity of deck material (ksi)

I = moment of inertia of beam (in^4)

e_g = distance between centers of gravity of basic beam and deck (in)

The distribution factor equation changes slightly when designing for moment with two or more design lanes loaded.

$$g = 0.075 + \left(\frac{S}{9.5}\right)^{0.6}\left(\frac{S}{L}\right)^{0.2}\left(\frac{K_g}{12.0Lt_s^3}\right)^{0.1} \tag{5}$$

The restrictions to the use of Equations (3) and (5) are that the girder spacing must be between 3.5 ft and 16 ft, the deck slab thickness must be between 4.5 in and 12 in, the span length must be between 20 ft and 240 ft, and there must be more than three girders.

The AASHTO LRFD Specifications specify the use of the lever rule for the exterior girder when one design lane is loaded. When more than one design lane is loaded, Table 4.6.2.2.2d-1 specifies the distribution factor be found with the equation:

$$g = eg_{interior} \tag{6}$$

where, $g_{interior}$ is the distribution factor for the interior girder and e is defined as:

$$e = 0.77 + \frac{d_e}{9.1} \tag{7}$$

with d_e being the width of the overhang, between -1.0 ft and 5.5 ft. A negative value of d_e indicates that the web is outboard of the curb or traffic barrier. For the live load tests performed on the Gills Creek Bridge, only one lane was loaded.

Girder Responses from Live Load Tests

In order to determine the girder distribution factors, the girder responses must first be determined. To get an idea of the accuracy of the instrumentation, example plots of the readings from the deflectometers, ER strain gauges, and WIM gauges on Span A in the 2004 tests are shown in Figure 17 through Figure 19. In Span A, the accuracy of the deflectometers was approximately ±0.001 in. The ER strain gauges had an accuracy of approximately ±8 µε, and the WIM gauges had an accuracy of approximately ±3 µε. For Span C, the deflectometers had an accuracy of approximately ±0.001 in. The ER strain gauges had an accuracy of approximately ±3 µε, and the WIM gauges had an accuracy of approximately ±0.5 µε. Note that the ER strain gauge on girder 1 did not work during the live load testing. Also, the WIM gauge on girder 2 was not reading accurate results, and a WIM gauge was not installed on girder 6.
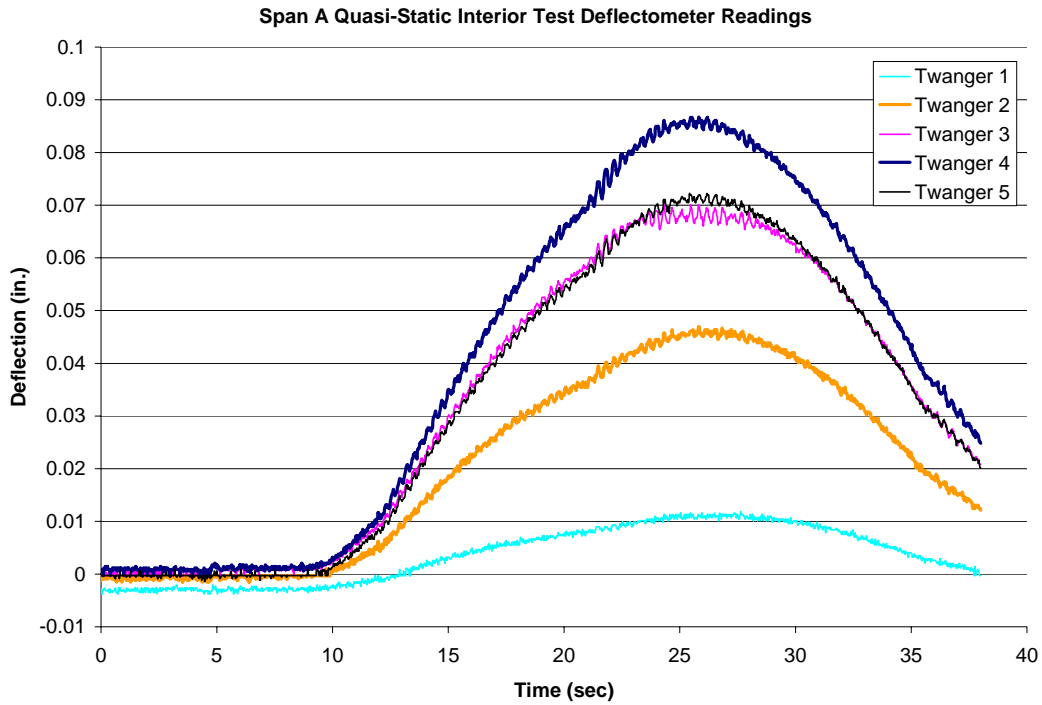
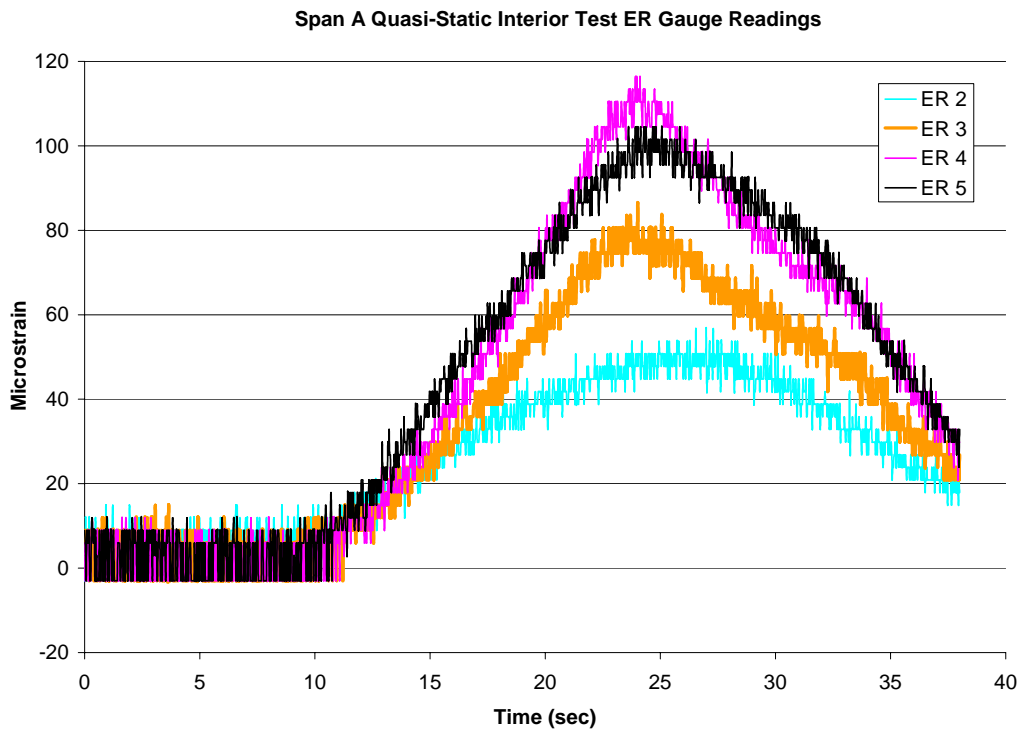**Figure 17. Example of Deflectometer Results for Span A**

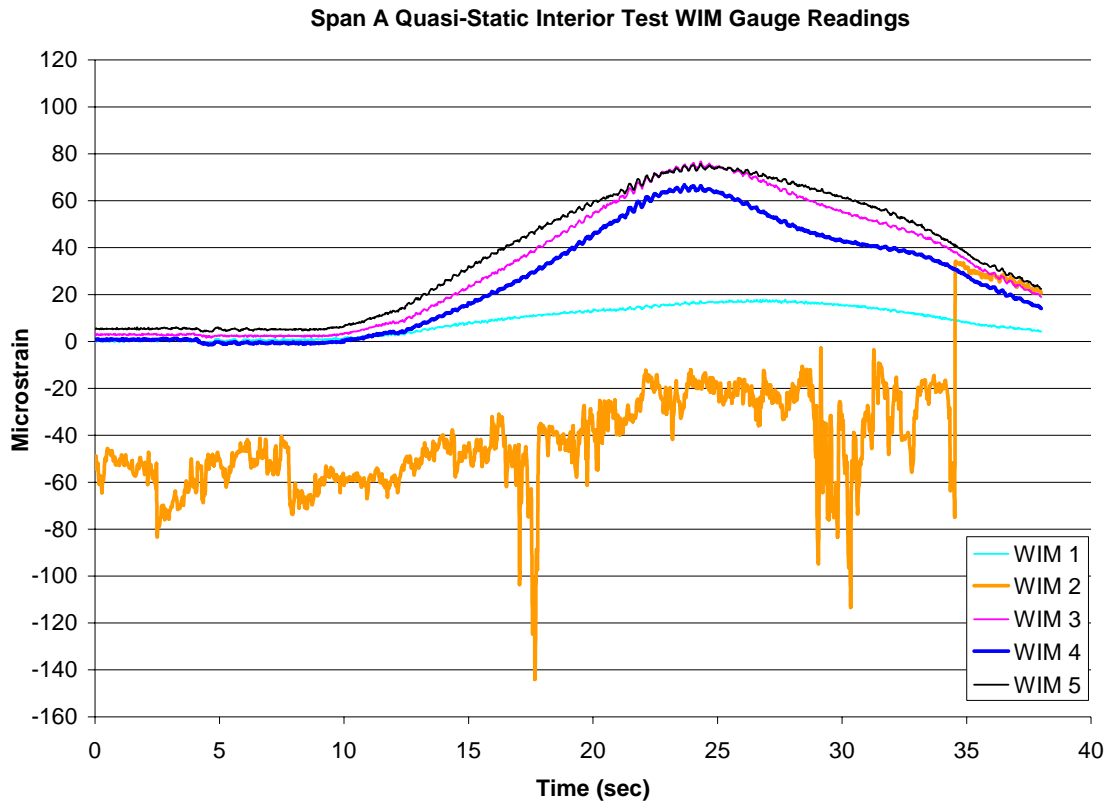**Figure 18. Example of ER Gauge Results for Span A**

Figure 19. Example of WIM Gauge Results for Span A

The average maximum deflections for Span A and Span C were compared for each truck orientation and for the 2003 and 2003 tests in Figure 20 through Figure 22. The deflections shown are the averages of the maximum deflections for all similar truck crossings. The girder deflections of Span A were higher than of Span C for all the truck orientations. The biggest deflection difference was from the dynamic live load tests. Span A and Span C also followed different trends. When the truck is traveling over the first interior girder (girders 4 and 9), it was expected that the girder with the highest deflection would be the girder under the truck. This was true for the interior orientation tests for Span A but not for Span C in both the dynamic and quasi-static tests. For the exterior orientation, both Spans A and C had the largest maximum deflection at the exterior girder under the truck location (girders 5 and 10).

25

Girder Deflections with Interior Truck Configuration - Dynamic
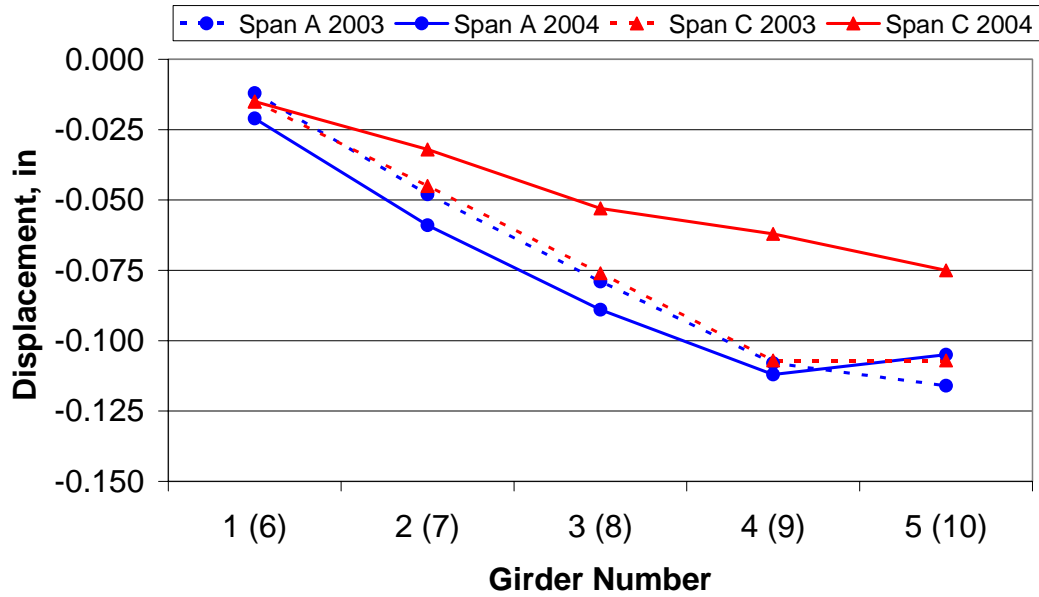
Figure 20. Comparison of Maximum Girder Deflections for Span A and Span C Under Dynamic Loads

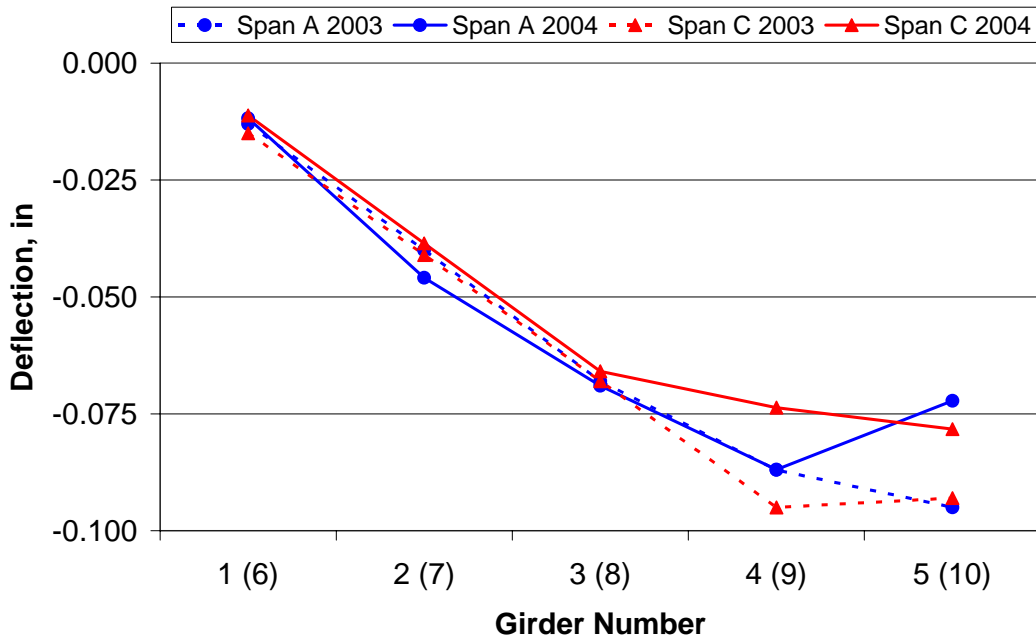**Girder Deflections with Interior Truck Configuration - Static**

Figure 21 Comparison of Maximum Girder Deflections for Span A and Span C Under Quasi-static Loads with Interior Truck Orientation

26

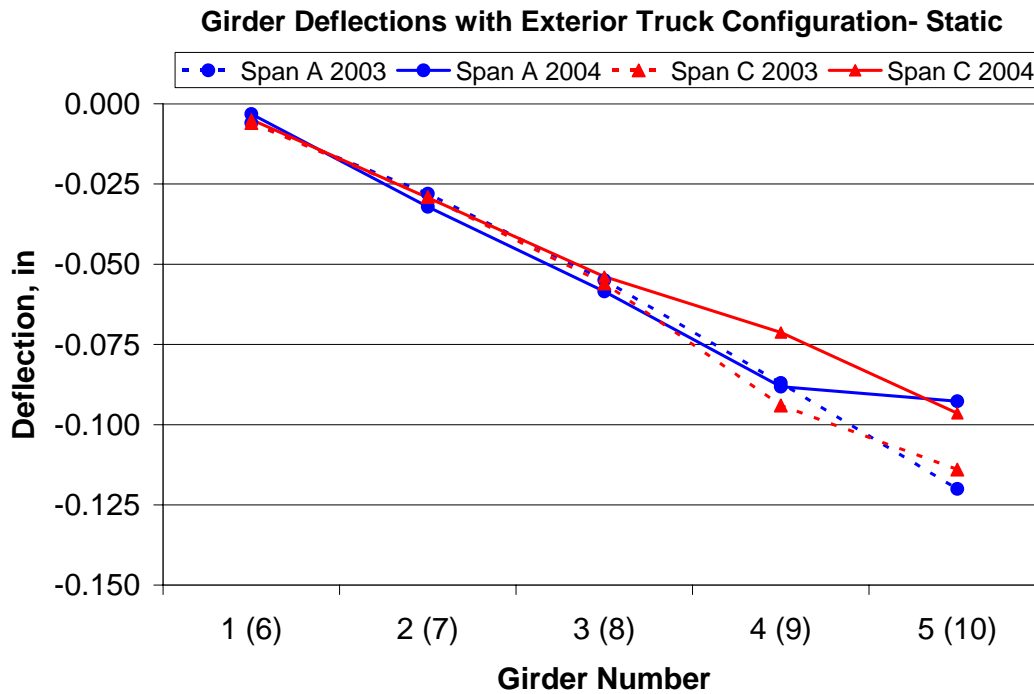**Girder Deflections with Exterior Truck Configuration- Static**

Figure 22. Comparison of Maximum Girder Deflections for Span A and Span C Under Quasi-static Loads with Exterior Truck Orientation

Figure 23 through Figure 25 compare the average maximum strains recorded by the ER strain gauges for Span A and Span C for each truck orientation in the 2004 tests. Similar to the deflection results, Span A experienced greater strains than Span C with the largest difference from the dynamic tests. For the ER gauges, the dynamic test showed the maximum strain to be highest at the exterior girder near the truck (girders 5 and 10). However, for the quasi-static interior orientation test, the maximum strain was at the first interior girder under the truck (girders 4 and 9). This could indicate the bridge deck works more as a plate when a dynamic load is applied causing the girders to respond in a linear fashion, making the highest strain in the exterior girder nearest the passing truck for both spans. When the truck is traveling more slowly, there is a more local influence, causing the greatest strain to be in the girder directly under the truck. Therefore, for the interior orientation, the highest strains were in girder 4 and 9 and for the exterior orientation, the highest strains were in girder 5 and 10. Note that the ER strain gauge installed on girder 1 was not operating at the time of the live load test so its maximum strain value was determined using a linear extrapolation from girders 2 and 3.

Figure 23. Comparison of Maximum Girder ER Strains for Span A and Span C Under Dynamic Loads

Figure 24. Comparison of Maximum Girder ER Strains for Span A and Span C Under Quasi-static Loads with Interior Truck Orientation

Span A vs Span C (Quasi-Static Test - Exterior) using ER Gauges

Figure 25. Comparison of Maximum Girder ER Strains for Span A and Span C Under Quasi-static Loads with Exterior Truck Orientation

The maximum WIM strains for Span A and Span C were compared for each truck orientation in Figure 26 through Figure 28. For the dynamic test, Span A had greater strains than Span C. The quasi-static tests had higher strains in Span A for girders 1 through 3 and in Span C for girders 9 and 10, the girders closest to the passing truck. Note that the WIM gauges on girders 2 and 6 were determined with linear interpolation. The WIM gauge on girder 2 was not reading accurate results (see Figure 19), and a WIM gauge was not installed on girder 6. Span C had a very different trend than Span A. Span C had more of a linear trend. In Span A, girder 4 seemed lower than expected for all three types of live load tests. This may be due to an error in installation or in the WIM gauge itself. All of the truck orientations produced the highest strain at the exterior girder near the truck path, except for in Span A for the quasi-static test with the interior truck orientation. In Span A for the quasi-static test with the interior truck orientation, the highest strains were at girders 3 and 5. The truck was straddling the first interior girder (girder 4) for this test. The high strains could be caused by the local response to the wheels that are near those two girders or, as noted earlier, there could be an error in the WIM gauge on girder 4. The average maximum strains measured by the WIM gauges are lower than the strains measured by the ER gauges. This is true for both the dynamic and the quasi-static tests.

Span A vs. Span C (Dynamic Test - Interior) using WIM Gauges
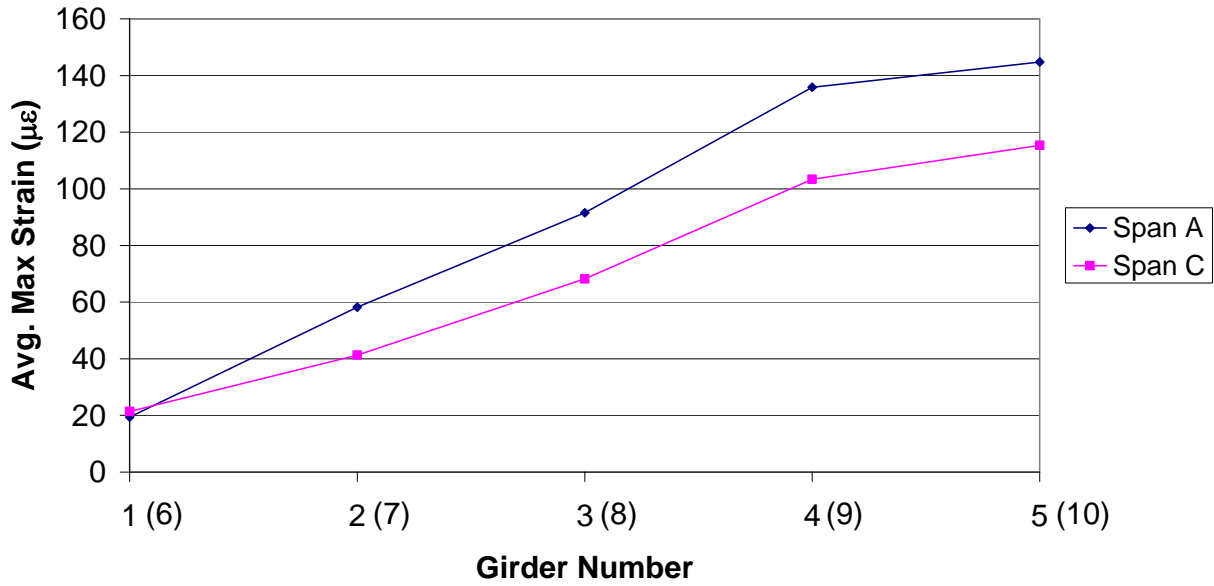

Figure 26. Comparison of Maximum Girder WIM Strains for Span A and Span C Under Dynamic Loads

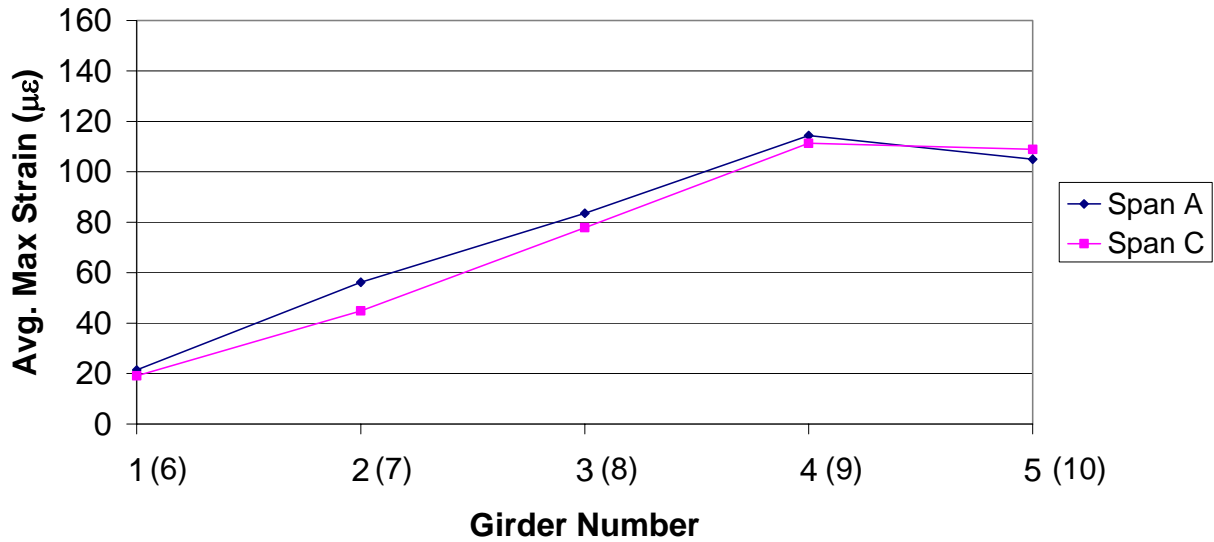**Span A vs. Span C (Quasi-Static Test - Interior) using WIM Gauges**

Figure 27. Comparison of Maximum Girder WIM Strains for Span A and Span C Under Quasi-static Loads with Interior Truck Orientation
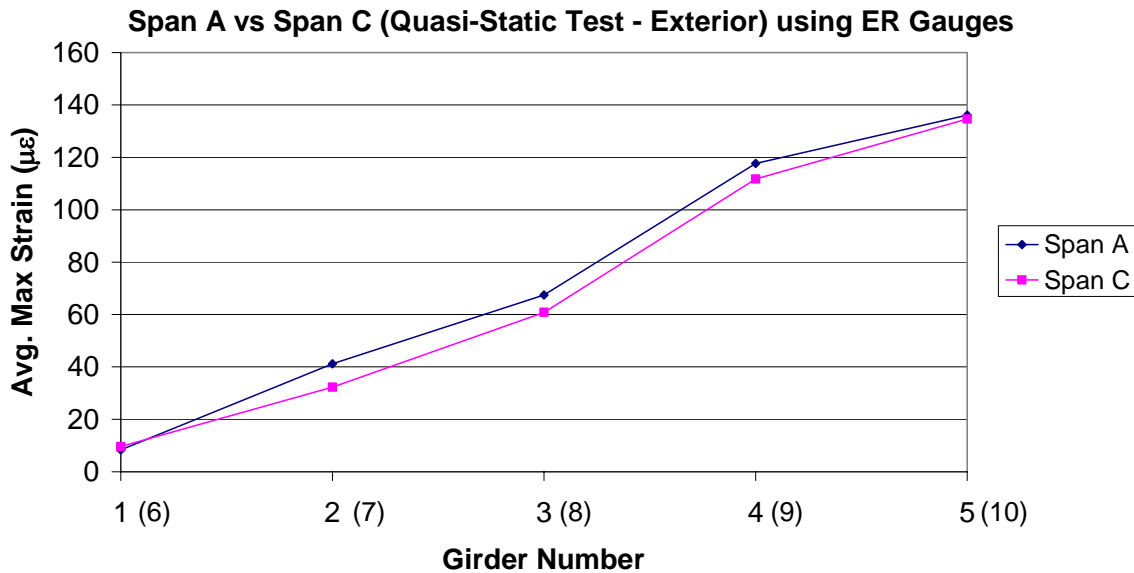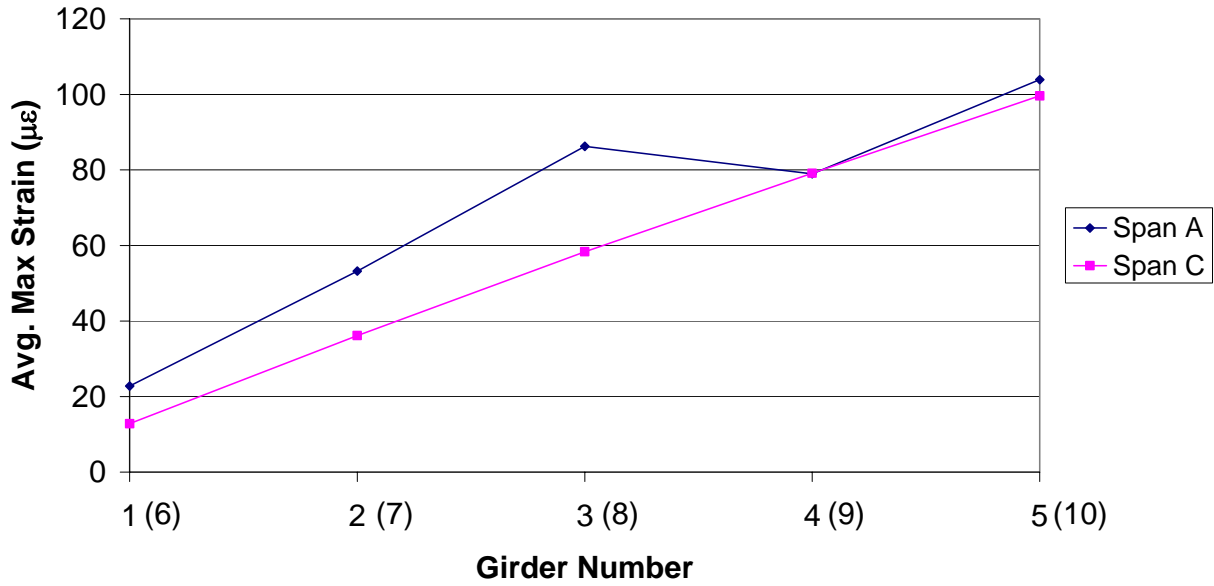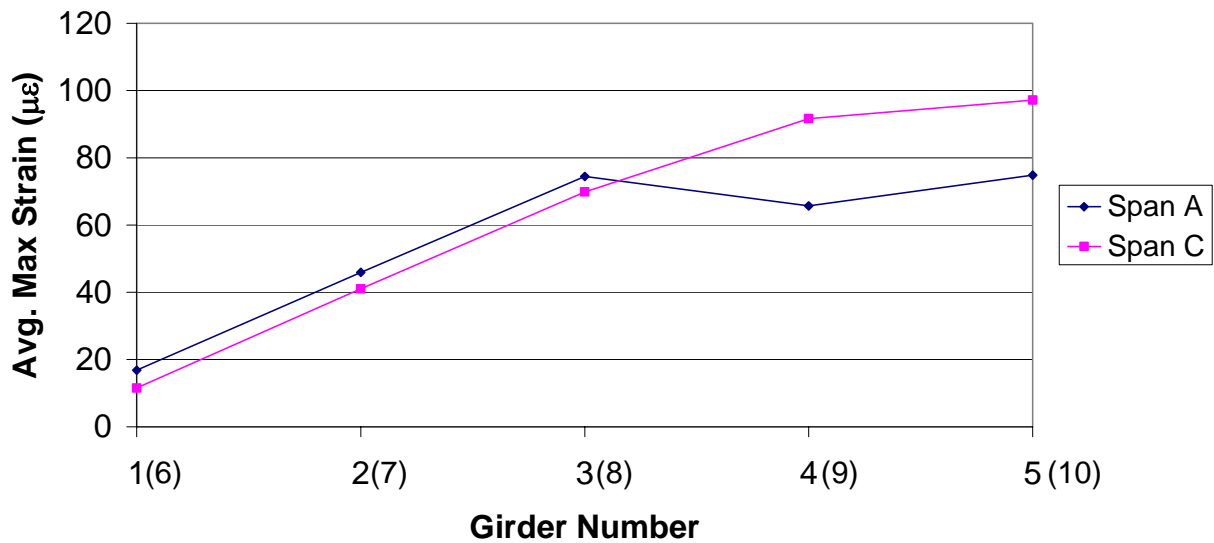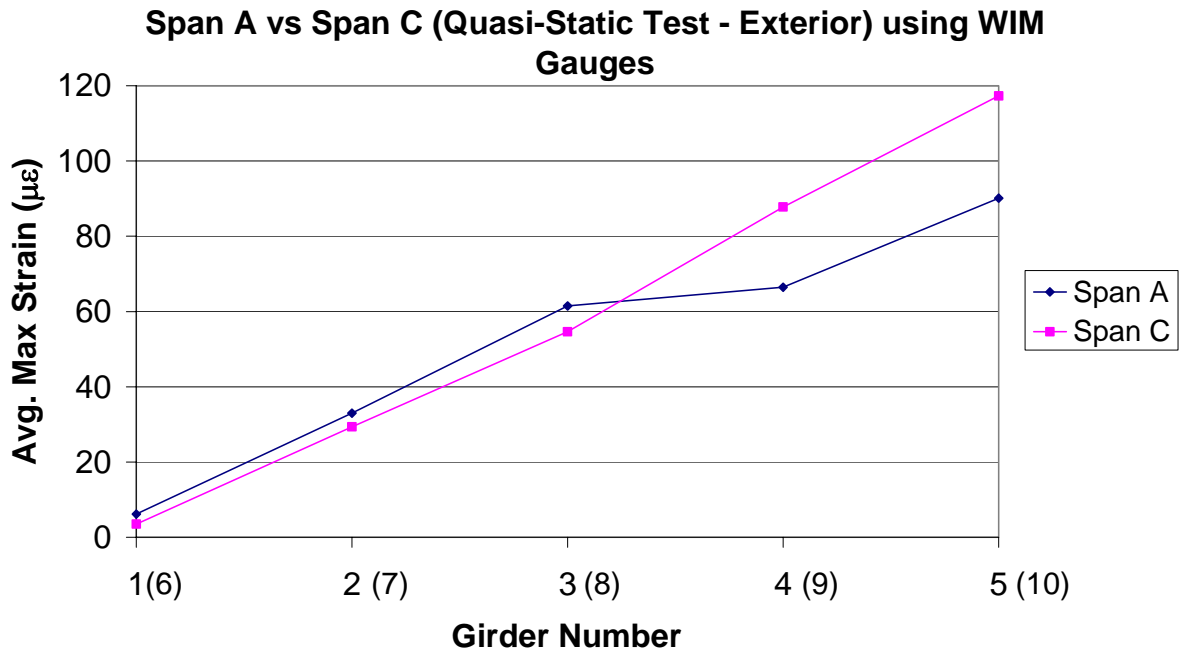
Figure 28. Comparison of Maximum Girder WIM Strains for Span A and Span C Under Quasi-static Loads with Exterior Truck Orientation

Determination of Girder Distribution Factors for Live Load Tests

The girder distribution factors were calculated using the data collected from the live load testing. Since the deck dimensions and girder locations along the length of the bridge remain constant, three sets of the data can be used to determine the distribution factors: the strain in the girders measured by the ER strain gauges, the strain in the girders measured by the WIM gauges, and the deflection of the girders measured by the deflectometers. In 2004, all three of these methods could be used since each girder was instrumented. However, in 2003, only deflections were used to determine GDFs. All of the live load tests were used for calculating the girder distribution factors

The procedure used to calculate the distribution factors was the same for each method and was carried out for each live load test. The procedure that was followed using the girder deflections is as follows. First, the maximum deflection of each girder was determined ($\Delta_{i,max}$). Secondly, the time of the highest $\Delta_{i,max}$ was recorded. Just like with the analysis of the transverse strains, the calculation is like taking a snapshot at the time of the maximum deflection. The deflection of each girder at the time of the highest $\Delta_{i,max}$ was recorded which is denoted as $\Delta_{corresp}$. Each girder's corresponding deflection was divided by the sum of all of the corresponding girder deflections to determine what fraction of the total deflection the girder is experiencing at the given time. This fraction is the girder distribution factor, referred to in AASHTO LRFD as *g*. For ease of comparison, the distribution factors were normalized by converting them into the denominator, D. To find D, the distribution factors were multiplied by two since there were two wheel lines and *g* is only for one wheel line.

31

A sample of the calculation of D from 2003 and 2004 can be seen in Table 2. The maximum deflections were recorded. In the 2004 example case, the maximum deflection of all the girders was the deflection at girder 4 at a time of 22.8 seconds, identified in bold print. The corresponding deflections at that time were recorded. Each corresponding deflection was divided by the sum of the corresponding deflections to get the girder distribution factor for each girder. Then to get the D value, the girder center-to-center spacing of 6.5 ft was divided by the GDF times two.

Table 2. Span A Quasi-Static Interior Configuration Sample GDF Data

	Deflections 2003					Deflections 2004				
	$\Delta_{I,max}$,in	Time, sec	$\Delta_{corresp.}$ in	GDF	"D"	$\Delta_{I,max}$,in	Time, sec	$\Delta_{corresp.}$ in	GDF	"D"
G1	0.0131	19.6	0.0127	0.043	76.1	0.0136	22.8	0.0113	0.039	82.4
G2	0.0422	19.6	0.0419	0.141	23.1	0.0479	22.8	0.0454	0.159	20.5
G3	0.0708	19.6	0.0705	0.237	13.7	0.0701	22.8	0.0689	0.241	13.5
G4	0.0856	19.6	0.0854	0.287	11.3	**0.0876**	22.8	0.0876	0.306	10.6
G5	**0.0873**	19.6	0.0873	0.293	11.1	0.0734	22.8	0.0734	0.256	12.7

For the 2004 tests, the girder distribution factors were calculated for each type of test using all three sources (deflectometers, ER strain gauges, and WIM gauges). To determine the GDF's, the deflections and strains of each girder need to be known. Some of the data needed to be interpolated to calculate the GDF's. For Span A, the ER strain gauge on girder 1 was inoperable so a linear relationship was used between the strains of girder 2 and 3 to find the strain in girder 1. The linear relationship was determined to be reasonable when examining the results of the deflectometers. A linear interpolation was also used to determine the WIM strain for girder 6. Girder 6 could not be instrumented since only nine WIM gauges were available. Interpolation was used for the WIM gauge on girder 2 since it did not have reasonable readings (see Figure 19). Fortunately, only one interpolation or less had to be used per GDF calculation. Table 3 through Table 8 show the GDF values that were calculated using the deflections of the girders only. The GDF value in bold print is the controlling girder distribution factor for the respective test. The GDF$_{avg}$ values for all five girders should sum to 1.0 when added together since they are fractions of the total load carried by the girder.

Table 3. GDF Results for Span A Interior Configuration Quasi-Static Tests

	Girder Distribution Factors from Deflection Data							
	2003				2004			
Girder #	Δ_{avg} , in	GDF$_{max}$	GDF$_{min}$	GDF$_{avg}$	Δ_{avg}, in	GDF$_{max}$	GDF$_{min}$	GDF$_{avg}$
G1	0.013	0.044	0.042	0.043	0.012	0.045	0.039	0.041
G2	0.040	0.141	0.130	0.133	0.046	0.165	0.159	0.161
G3	0.068	0.237	0.223	0.226	0.069	0.245	0.239	0.241
G4	0.087	0.287	0..285	**0.286**	0.087	0.306	0.302	**0.304**
G5	0.095	0.320	0.293	0.313	0.073	0.256	0.249	0.253
			$\Sigma =$	1.000			$\Sigma =$	1.000

Table 4. GDF Results for Span A Interior Configuration Dynamic Tests

	Girder Distribution Factors from Deflection Data						
	2003				**2004**		
Girder #	Δ_{avg}, in	**GDF$_{max}$**	**GDF$_{min}$**	**GDF$_{avg}$**	Δ_{avg}, in	**GDF$_{max}$**	**GDF$_{min}$**	**GDF$_{avg}$**
G1	0.012	0.044	0.024	0.033	0.021	0.056	0.037	0.049
G2	0.048	0.142	0.125	0.132	0.059	0.161	0.140	0.153
G3	0.079	0.224	0.212	0.218	0.089	0.237	0.227	0.232
G4	0.108	0.303	0.288	0.296	0.112	0.304	0.287	**0.294**
G5	0.116	0.332	0.305	**0.320**	0.105	0.291	0.261	0.273
			$\Sigma =$	1.000			$\Sigma =$	1.000

Table 5. GDF Results for Span C Interior Configuration Quasi-StaticTests

	Girder Distribution Factors from Deflection Data						
	2003				**2004**		
Girder #	Δ_{avg} , in	**GDF$_{max}$**	**GDF$_{min}$**	**GDF$_{avg}$**	Δ_{avg} , in	**GDF$_{max}$**	**GDF$_{min}$**	**GDF$_{avg}$**
G6	0.015	0.052	0.047	0.049	0.012	0.045	0.039	0.042
G7	0.041	0.132	0.129	0.131	0.039	0.150	0.138	0.144
G8	0.068	0.217	0.216	0.217	0.066	0.252	0.241	0.246
G9	0.095	0.307	0.304	**0.305**	0.074	0.279	0.272	0.275
G10	0.093	0.302	0.294	0.298	0.078	0.304	0.281	**0.293**
			$\Sigma =$	1.000			$\Sigma =$	1.000

Table 6. GDF Results for Span C Interior Configuration Dynamic Tests

	Girder Distribution Factors from Deflection Data						
	2003				**2004**		
Girder #	Δ_{avg}, in	**GDF$_{max}$**	**GDF$_{min}$**	**GDF$_{avg}$**	Δ_{avg} , in	**GDF$_{max}$**	**GDF$_{min}$**	**GDF$_{avg}$**
G6	0.015	0.053	0.033	0.042	0.015	0.069	0.057	0.062
G7	0.045	0.135	0.122	0.129	0.032	0.146	0.117	0.130
G8	0.076	0.220	0.214	0.217	0.053	0.231	0.217	0.226
G9	0.107	0.311	0.300	**0.306**	0.062	0.264	0.248	0.255
G10	0.107	0.321	0.296	0.306	0.075	0.353	0.307	**0.326**
			$\Sigma =$	1.000			$\Sigma =$	1.000

Table 7. GDF Results for Span A Exterior Configuration Quasi-StaticTests

	Girder Distribution Factors from Deflection Data						
	2003				**2004**		
Girder #	Δ_{avg}, in	**GDF$_{max}$**	**GDF$_{min}$**	**GDF$_{avg}$**	Δ_{avg} , in	**GDF$_{max}$**	**GDF$_{min}$**	**GDF$_{avg}$**
G6	0.006	0.022	0.016	0.019	0.004	0.015	0.008	0.012
G7	0.028	0.097	0.090	0.094	0.033	0.120	0.116	0.117
G8	0.055	0.188	0.184	0.187	0.059	0.215	0.210	0.213
G9	0.087	0.295	0.293	0.294	0.089	0.322	0.319	0.321
G10	0.120	0.414	0.400	**0.407**	0.093	0.340	0.336	**0.338**
			$\Sigma =$	1.000			$\Sigma =$	1.000

Table 8. GDF Results for Span C Exterior Configuration Quasi-StaticTests

Girder #	\(\Delta_{avg}\), in	GDF$_{max}$	GDF$_{min}$	GDF$_{avg}$	\(\Delta_{avg}\), in	GDF$_{max}$	GDF$_{min}$	GDF$_{avg}$
		2003				**2004**		
G6	0.006	0.020	0.018	0.019	0.006	0.026	0.015	0.019
G7	0.029	0.098	0.096	0.097	0.030	0.116	0.112	0.114
G8	0.056	0.190	0.187	0.189	0.054	0.212	0.209	0.211
G9	0.094	0.316	0.314	0.315	0.072	0.282	0.275	0.279
G10	0.114	0.384	0.377	**0.380**	0.096	0.380	0.374	**0.377**
			Σ =	1.000			Σ =	1.000

The GDF and D values for Span A calculated from the deflections of the girders are presented in Table 9. Table 10 shows the same calculations for Span C. The D value is the denominator of equation 4, $g = S/D$.

Table 9. GDF's and D-values for Span A from Deflection Data

				Span A						
				GDF's (per axle)			Denominator "D" (per wheel)			
Year	Truck Config	Type	# Passes	Min	Max	Avg.	Min	Max	Avg.	Comb. Avg.
2003	Interior	Quasi-Static	5	0.285	0.287	0.286	11.4	11.3	11.4	11.2
		Dynamic	6	0.288	0.303	0.296	11.3	10.7	11.0	
	Exterior	Quasi-Static	5	0.400	0.414	0.407	8.1	7.9	8.0	8.0
2004	Interior	Quasi-Static	5	0.302	0.306	0.304	10.8	10.6	10.7	10.9
		Dynamic	6	0.287	0.304	0.294	11.3	10.7	11.1	
	Exterior	Quasi-Static	5	0.336	0.340	0.338	9.7	9.6	9.6	9.6

Table 10. GDF's and D-values for Span C from Deflection Data

				Span A						
				GDF's (per axle)			Denominator "D" (per wheel)			
Year	Truck Config	Type	# Passes	Min	Max	Avg.	Min	Max	Avg.	Comb. Avg.
2003	Interior	Quasi-Static	5	0.304	0.307	0.305	10.7	10.6	10.7	10.6
		Dynamic	6	0.300	0.311	0.306	10.8	10.5	10.6	
	Exterior	Quasi-Static	5	0.377	0.384	0.380	8.6	8.5	8.6	8.6
2004	Interior	Quasi-Static	5	0.272	0.279	0.275	11.9	11.7	11.8	12.3
		Dynamic	6	0.248	0.264	0.255	13.1	12.3	12.7	
	Exterior	Quasi-Static	5	0.374	0.380	0.377	8.7	8.5	8.6	8.6

The process of determining the GDF's and the "D" factors was also carried out using the strains recorded by the ER gauges and the WIM gauges. Figure 29 shows a graphical representation of the "D" factor for both the 2003 and 2004 live load testing. For the interior configuration, the quasi-static and dynamic "D" values were averaged together to get a combined average as shown in Table 11 and Table 12. The AASHTO Standard Specification Interior distribution factor of S/7.0, AASHTO LRFD Interior factor of S/7.4, and AASHTO Exterior distribution factor of S/6.5 for one lane loaded are also included in Figure 28 for comparison to the recorded results. For ease of comparison, the AASHTO LRFD distribution factor was converted from a fraction of a lane load to a wheel line. The calculations of the AASHTO LRFD distribution factors and the intermediate results for the ER strain gauges and WIM gauges can be found in Phillips (2004). Note that a larger D value corresponds to a smaller GDF.
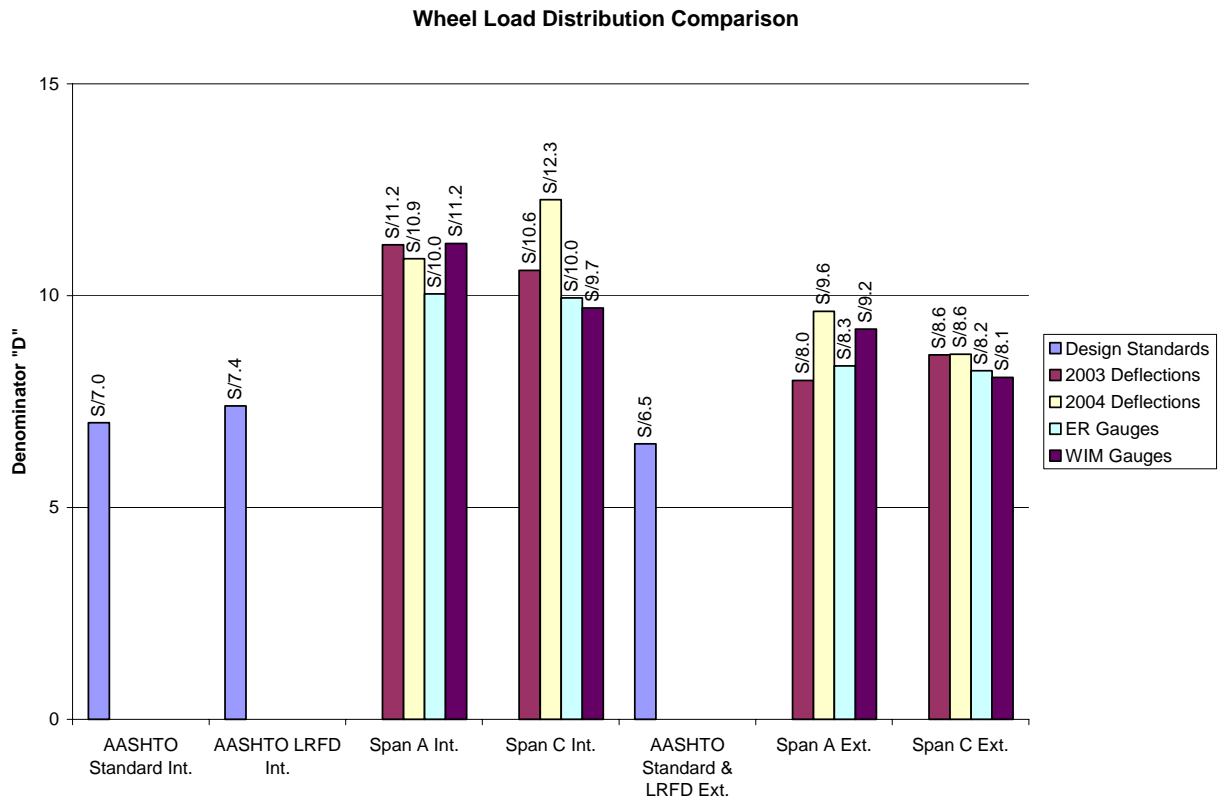
Wheel Load Distribution Comparison

Figure 29. Distribution Factor Comparison

For the interior girder, the distribution factors determined for Span A and Span C do not vary significantly. Using the deflections, the GDF determined for Span A was greater than for Span C, S/10.9 versus S/12.3. The GDF's determined for Span A and C using the ER strains were the same at S/10.0. Finally, the GDF values from the WIM strains are smaller for Span A than Span C, S/11.2 versus S/9.7. With the GDF values determined from the three methods, it is unclear if Span A has a higher or lower distribution factor than Span C for the interior girder orientation. However, all the GDF's for both Span A and C were less than the design values of S/7.0 from the AASHTO Standard and S/7.4 from the AASHTO LRFD, indicating that the interior girders are taking a smaller fraction of the load than designed for.

For the exterior girder, the calculated GDF's for Span A are slightly less than for Span C using all three methods, with S/9.6 versus S/8.6 using deflections, S/8.3 versus S/8.2 using ER strains, and S/9.2 versus S/8.1 using WIM strains. All of these values were less than the design limit of S/6.5 calculated using the lever rule.

When comparing the distribution factors from the live load tests performed in 2004 to those from 2003, there is no clear trend in the changes. For the interior girder orientation, the GDF of 2003 for Span A is slightly lower than for Span C. However, the values of S/11.2 for Span A and S/10.6 for Span C are very similar to the values recorded in 2004. This indicates that there was no significant change in the distribution factors over the year between live load tests. The 2003 GDF values for the exterior girder orientation show a trend contrary to the 2004 results. In 2003, Span A had a higher GDF than Span C, S/8.0 versus S/8.6. The 2004 GDF values for Span A were lower than Span C. Like the interior orientation values, the GDF from 2003 was very close to the GDF's from 2004 for the exterior orientation.

The quasi-static and dynamic GDF's were averaged for each span to compare the spans. In the year 2004, the average GDF for the interior configuration of Span A was S/10.9 and for Span C was S/12.25. That equates to GDF's of 0.596 for Span A and 0.531 for Span C, a difference of 6.6% of the total load per wheel line. The GDF difference for 2003 was 3.0%. Although, the 2004 difference is more than twice that calculated for 2003, 6.6% is still a small difference. The deck should be monitored in later years to see if the difference continues to increase but for now the GDF's are within the design limits and do not vary enough to be alarming. It can be concluded from the comparison of Span A and C that the distribution factors calculated from the girder deflections for the deck reinforced with GFRP and epoxy-coated steel are the same as the deck reinforced with all epoxy-coated steel. This is only true since the girder spacing, girder properties, and deck properties are constant.

Comparisons between the distribution factors of the two spans were also made using the information obtained from the ER strain gauges and the WIM gauges. Only data from the live load testing in 2004 was used since only three girders were equipped with ER strain gauges and WIM gauges in 2003. The average distribution factors are displayed in Figure 29. The average distribution factors for the interior orientation determined using the ER strains for are identical at S/10.0 for Span A and for Span C. The exterior orientation resulted in nearly identical average GDF's for Span A and Span C with S/8.3 and S/8.2, respectively.

The average distribution factors determined with the WIM strains had the most variation. The difference between the two spans is the difference between the average of Span A, S/11.2, and the average of Span C, S/9.7. That is equivalent to 0.578 and 0.667, a difference of 8.9%. The difference indicates that the first interior girder in Span C is carrying 8.9% more of the total load per wheel line than in Span A. The difference is significant; however, the values are well within the distribution design requirements from the AASHTO Standards of S/7.0 (0.929) and from the AASHTO LRFD of S/7.4 (0.878). The difference may be due to an inaccuracy in the WIM gauges. Also, the questionable WIM gauge readings for girder 4 in Span A could influence the results. For all the methods, the average distribution factors calculated for the exterior orientation were very similar between Span A and C.

Dynamic Load Allowances

Introduction and AASHTO Definitions

Another design factor that needs to be considered is the dynamic load allowance, or impact factor (IM). The load imposed on a bridge structure is influenced by the speed at which the vehicle is traveling. With increased speed, the load being applied increases as well. The dynamic load allowance quantifies this phenomenon. The dynamic load allowance is influenced by how level and smooth the roadway is. This means that any imperfections in the deck surface, bumps in the roadway, or settlement of the joints or abutments change the dynamic load allowance value.

The AASHTO Standard Specification defines the IM as:

$$I = 50/(L+125) \qquad\qquad (8)$$

where I = impact factor (cannot exceed 30%)
        L = length of portion of slab that is loaded to produce the maximum stress in member (ft).

The Gills Creek bridge has a span of 45 ft, so the IM would be $I = 50/(45+125) = 29\%$. AASHTO LRFD Specifications specifies in Table 3.6.2.1-1 that for all bridge components other than deck joints, and for all limit states other than fatigue and fracture, the IM is 33%.

Determination of Dynamic Load Allowances from Live Load Tests

Dynamic load allowances were calculated for both the 2003 and 2004 tests using the strain in the girders measured by the ER strain gauges, the strain in the girders measured by the WIM gauges, and the deflection of the girders measured by the deflectometers. Only the live load tests done over the interior girder were used since no dynamic tests were performed over the exterior girder due to safety reasons.

The procedure used to calculate IM was the same for each method and was as follows. The baseline quasi-static and dynamic girder response (deflection or strain) of each test was determined by averaging the first five readings recorded. These readings are representative of the deflection or strain in the girder before the truck is on the span. Then, for each quasi-static and dynamic test, the maximum girder response was recorded. The base line response was subtracted from the maximum to get the calculated response from each test. Example calculations are presented in Phillips (2004) and Harlan (2004).

For all the cases, the IM values for girder 5 and girder 10 will be examined. In the 2004 tests, the average of the maximum deflection of girder 5 under the quasi-static live load was 0.073 in. The maximum deflections caused by the dynamic live load ranged from 0.099 in to 0.112 in. Figure 30 shows a comparison of a quasi-static and dynamic response versus time for girder 5 of Span A. The plot illustrates how the girders deflect more when a truck is going faster than when it is going slower, demonstrating the concept of dynamic load allowance. Figure 31 shows a comparison of a quasi-static and dynamic response versus time for girder 10 of Span C.
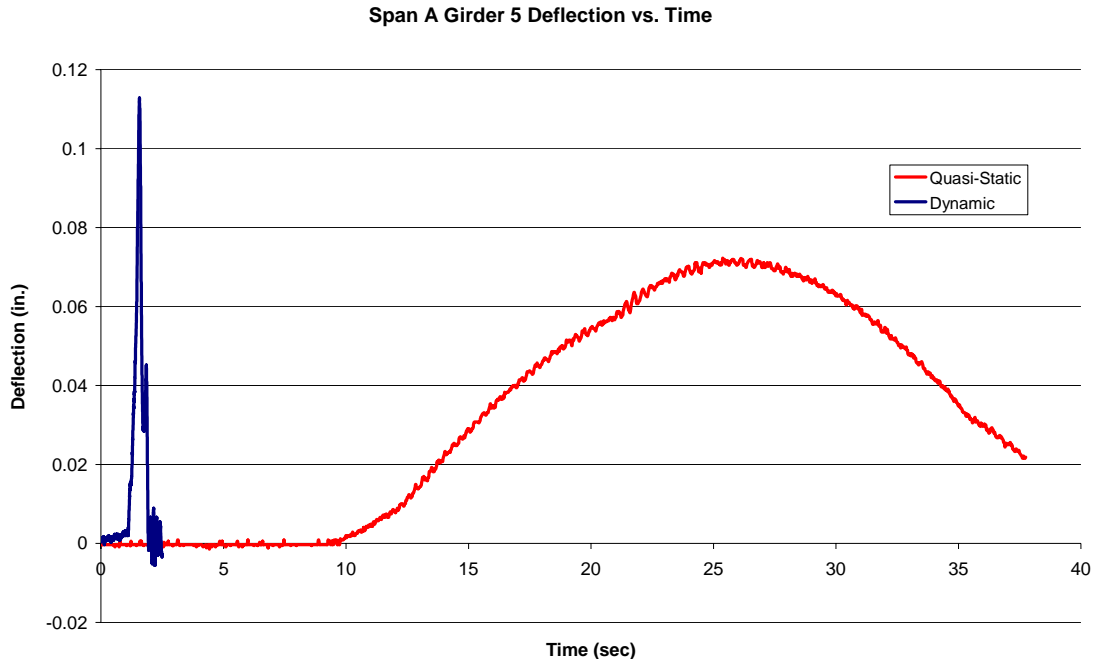
Span A Girder 5 Deflection vs. Time

Figure 30. Span A Deflections Under Quasi-static and Dynamic Loading

The average Dynamic Load Allowances (IM) were calculated by dividing the average of the maximum dynamic deflections for the given truck direction by the average deflection in the Quasi-Static tests and then subtracting 1 to get the percentage increase. Figure 32 presents a summary of the Dynamic Load Allowances for both spans and both years of testing. From the figure it can be seen that for Span A in 2004, the Dynamic Load Allowance using deflections was 0.52 for northbound and 0.37 for southbound. The design IM value from the AASHTO Standard was 0.29 and from the AASHTO LRFD was 0.33. Neither of the measured IM values were within the AASHTO requirements. The average Dynamic Load Allowance calculated for girder 10 in Span C was 0.16 for northbound and 0.31 for southbound. These values were within the AASHTO LRFD limits, however the southbound value was slightly higher than the AASHTO Standard limit of 0.29.

In all cases, the IM values calculated in 2004 were higher than in 2003. The 2004 values in Span A, both southbound and northbound, exceed the limits of the AASHTO Standard and LRFD. Even in 2003 the northbound tests of Span A had IM values that exceeded the limits. One explanation of the increase in IMs is increased flexibility of the bridge deck. With more flexibility, higher loads can create greater responses in the girders. As stated earlier, no visible cracking of the bridge deck was detected. In Span A, the northbound IM values were higher than the southbound. When the truck was traveling northbound onto Span A, it was going over the abutment onto the first span of the bridge. In Span C, the trend was opposite with the southbound IM values being higher. When the truck was traveling southbound onto Span C, it was going over the abutment onto the first span of the bridge. The abutments may cause the IM values to be higher by influencing how the truck load is distributed when traveling at a high speed. Cracking was observed at the approach but no settling.
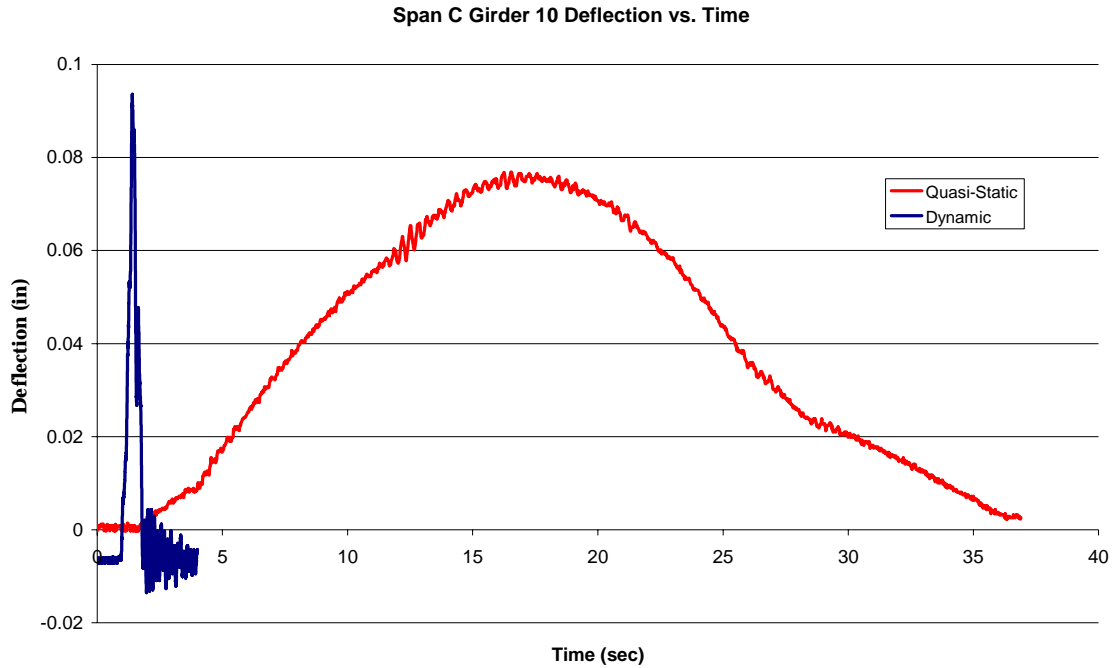
Span C Girder 10 Deflection vs. Time

Figure 31. Span C Deflections Under Quasi-static and Dynamic Loading

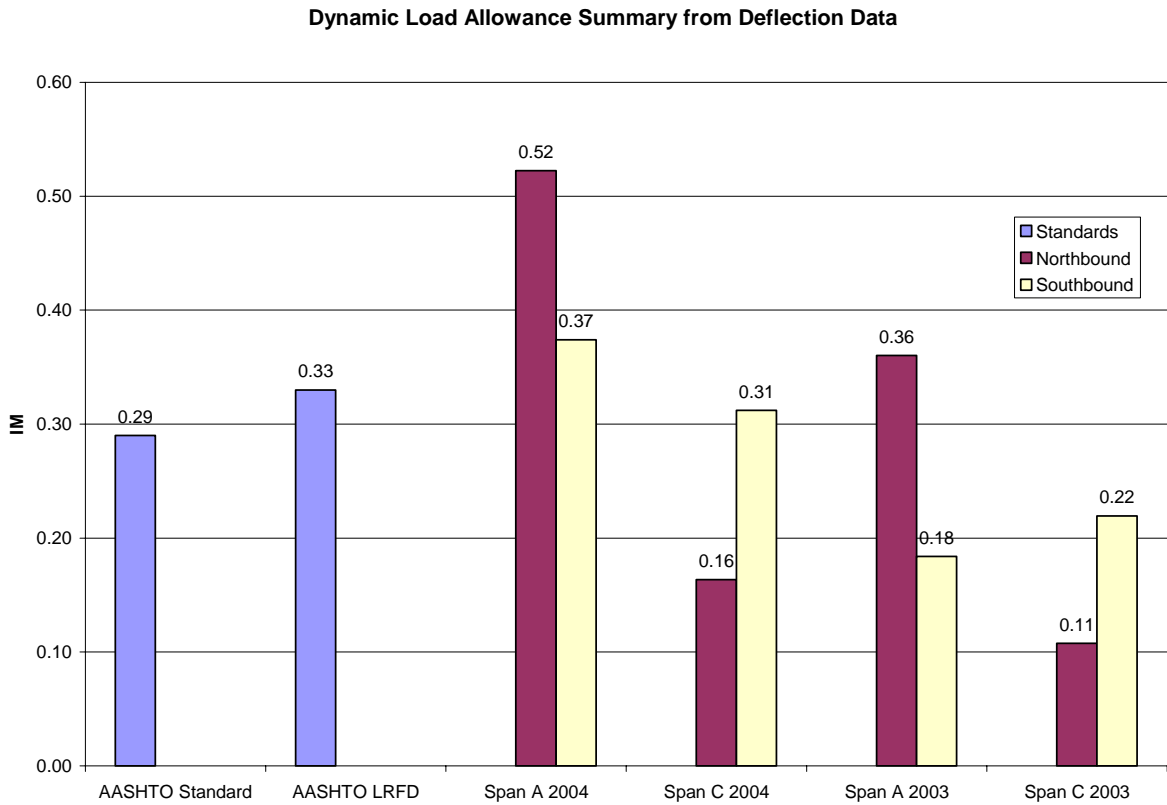**Dynamic Load Allowance Summary from Deflection Data**

Figure 32. Dynamic Load Allowance Summary for Deflection Data

For comparison, Figure 33 shows the IM values calculated from the ER strain gauges in Span A (girder 5) and Span C (girder 10). The extremely low strains under the dynamic loads for Span A in the 2003 tests were concluded to be erroneous. The IM values calculated from the WIM strain gauges on girders 5 and 10 are shown in Figure 34. There is no WIM strain data from the 2003 live load test to compare to. For both the ER and WIM gauges, the results from 2004 indicate that Span A has IM values that are above the design impact factors of AASHTO. All three methods used to determine the IM values indicate that Span A has a higher dynamic load allowance than the value used in design. The results for Span C are within the design values.

It is important to note that although the impact factors were above the design values, there was no cracking or unusual response of the structure seen during testing. The girders are Grade 50, so they have a minimum tensile strength of 50 ksi. The highest strain recorded in the girders of Span A was 159.4 $\mu\varepsilon$. The strain is converted to stress using $\sigma=E_s\varepsilon$, where E_s is the modulus of elasticity of the steel, 29,000 ksi. The maximum stress in the girders of Span A was calculated to be $29,000*(159.4*10^{-6})$ or 4.62 ksi. The stresses in the steel girders were less than 10% of the tensile strength of the girder. For Span C, the stresses in the girders were even smaller.
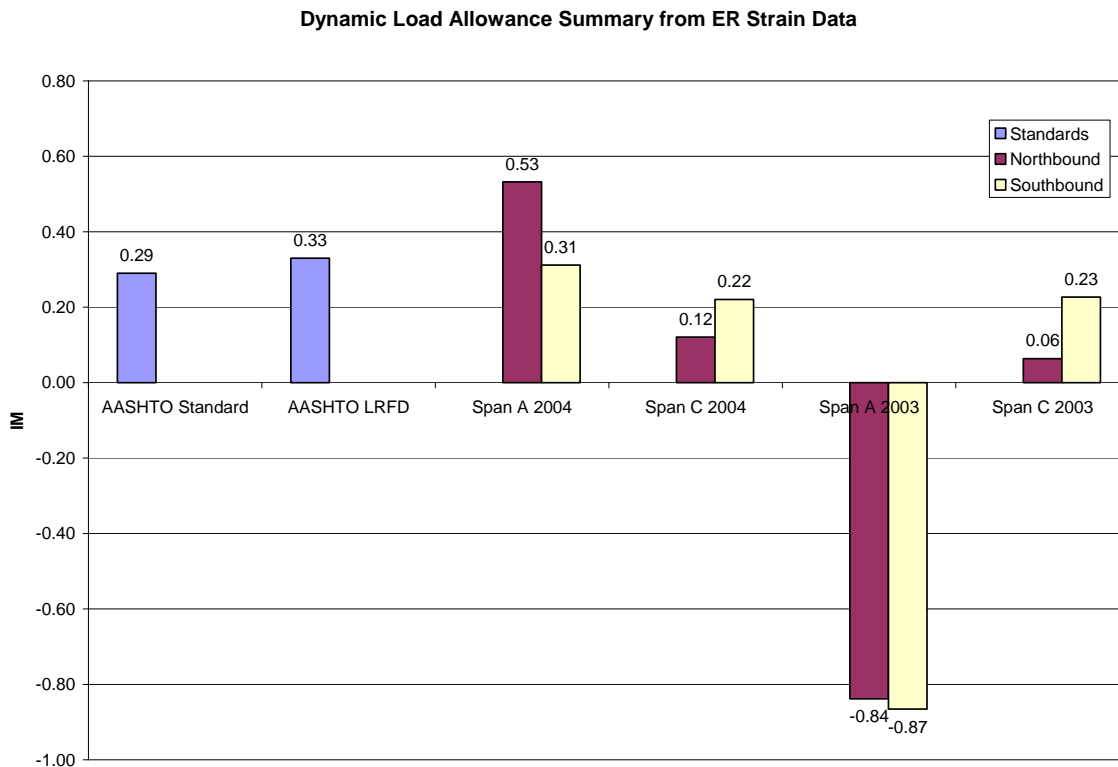

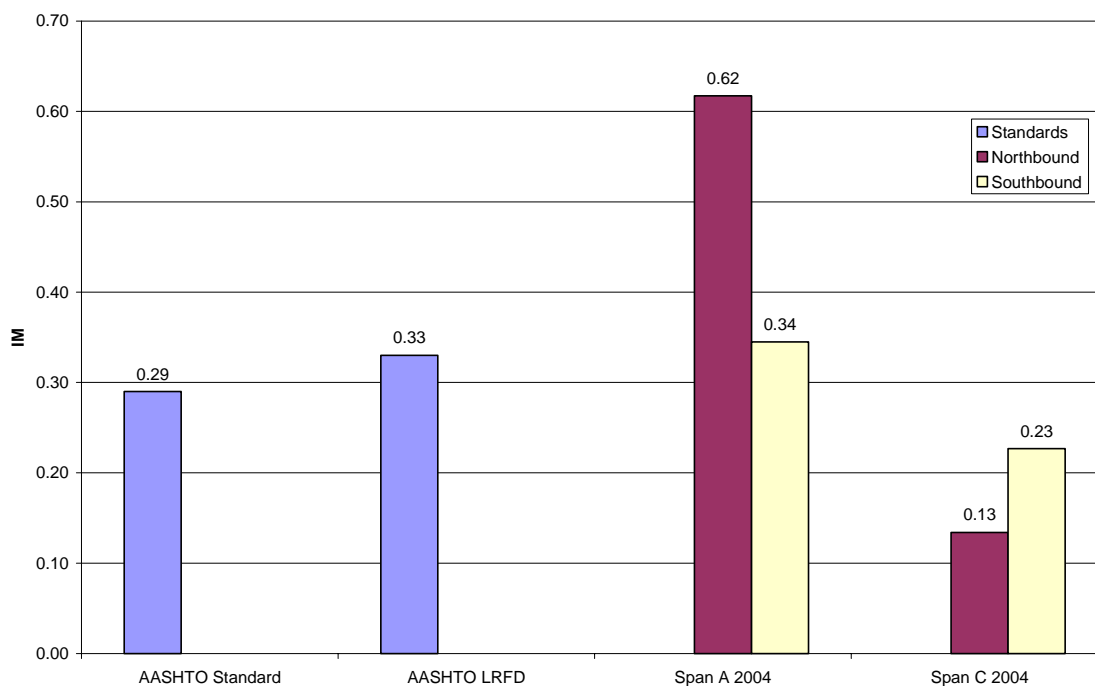**Figure 33. Dynamic Load Allowance Summary for ER Strain Data**

Figure 34. Dynamic Load Allowance Summary from WIM Strain Data

Long-term Observations

Span A of the Gills Creek Bridge was monitored from November 20, 2003, to November 1, 2004, approximately 1 year (347 days). The instrumentation in the bridge deck was connected to a long-term data acquisition system, and readings were taken every hour. The 24 readings from each day were averaged to get the daily average to illustrate the trends more easily. At the time of installation, there were 17 ER strain gauges, six VW gauges, and six thermocouples still working properly.

Temperatures

Temperatures were recorded by two types of instrumentation: thermocouples and thermisters. The thermocouples are at two locations, half way between girders 4 and 5 near the abutment and near midspan. At each location, there is a thermocouple at the top, middle, and bottom of the deck. The thermisters are in the VW gauges that are in three locations, at the abutment over girder 4, at midspan over girder 4, and at midspan over girder 5. A thermister is at the top and bottom of the deck at each location. The exact locations can be seen in Figure 4. All of the temperature instrumentation operated correctly throughout the year except for the middle thermocouple at the midspan (TMM). TMM began not taking readings every hour on day 59, and then stopped working completely on day 127. Figure 35 shows a plot of the temperature recorded by the thermocouple at the abutment of Span A in the top of the deck (TAT).
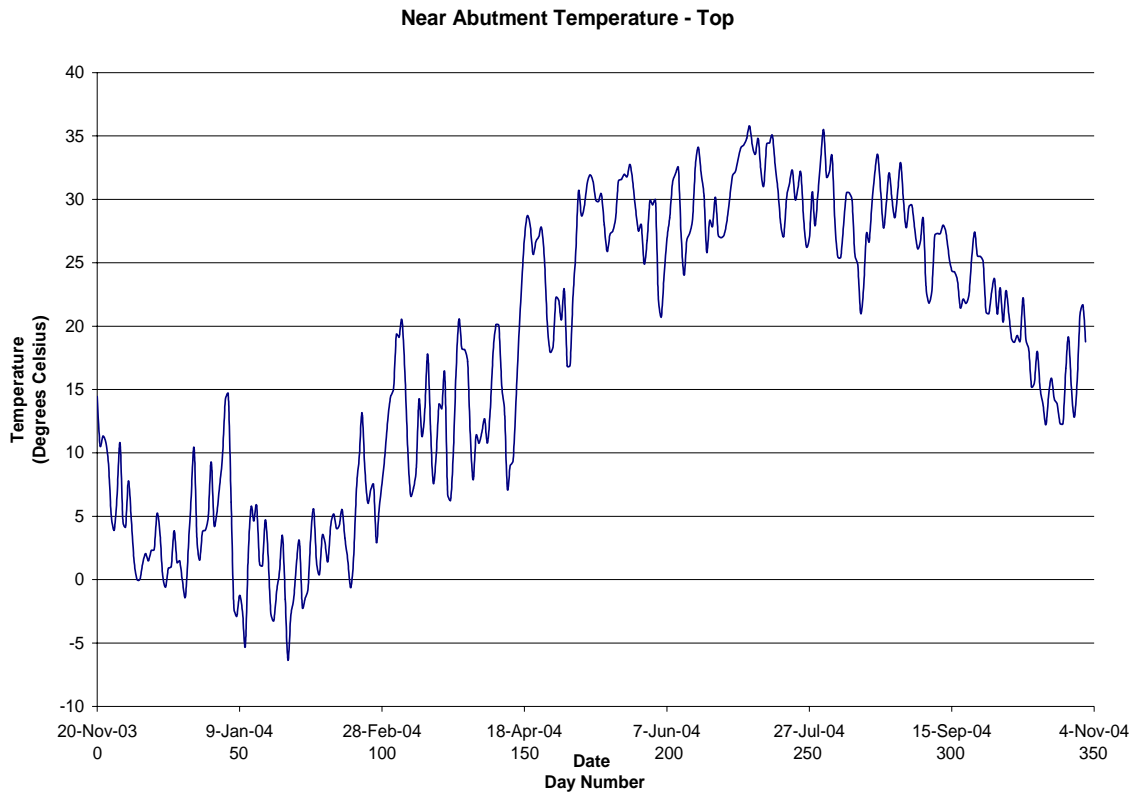
Near Abutment Temperature - Top

Figure 35. TAT Long-term Readings

All of the thermocouples had similar readings. There was very little difference between the top deck temperature at the abutment and at the midspan, no more than one degree Celsius. The bottom of the deck at midspan was always slightly warmer than at the abutment; never more than one degree Celsius. At a given location, the top of the deck was usually the warmest. The middle thermocouple read a temperature somewhere in between the top and bottom thermocouples. To illustrate this relationship, the temperatures near the abutment are examined. To see the differences, the bottom temperature was subtracted from the top temperature and from the middle temperature. In Figure 36, the bottom temperature is represented by $x = 0$ since it was used as the baseline for comparison. The middle temperature was always between the top and bottom temperatures. The difference between the bottom and the top temperature was rarely more than 1.5°C.
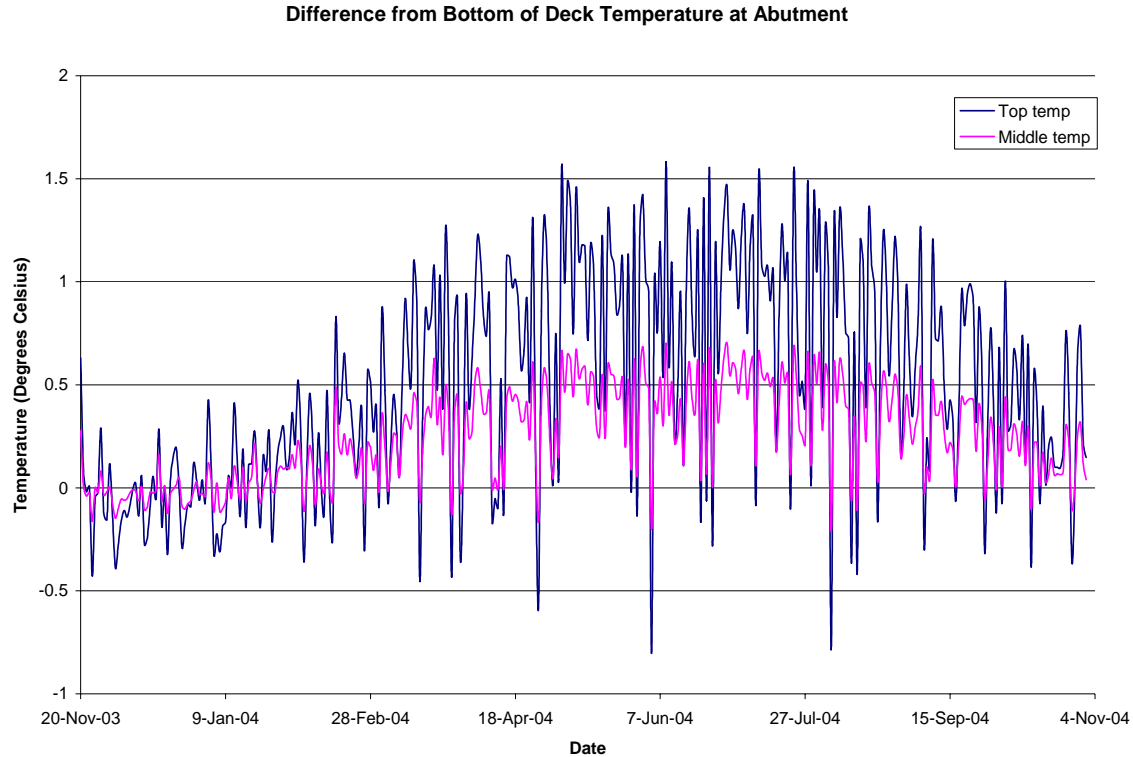
42

Figure 36. Comparison of Deck Temperatures at Abutment

Comparing the temperatures recorded at the abutment by the thermocouples and by the thermisters, the thermocouples read a little higher than the thermisters at both the top and the bottom of the deck. This could be due to the positioning of the thermocouple, with the thermocouple located half way between girders 4 and 5 and the thermister over girder 4. The temperatures at the top of the slab recorded by the two instruments are plotted in Figure 37. The measurements from the bottom of the slab were also very close to one another.

The trends at midspan are similar to the abutment. For both the top and bottom of the deck at midspan, the thermocouple tended to record a slightly higher temperature than the thermisters. The thermister over girder 4 gave higher readings than girder 5. This may be attributed to the parapet being so close to girder 5 and keeping the deck cooler in that location.

The temperature readings of the thermocouples and the thermisters correspond well. It can be concluded from the comparisons of the temperature readings that they all are very similar and, therefore, validate each other's accuracy.
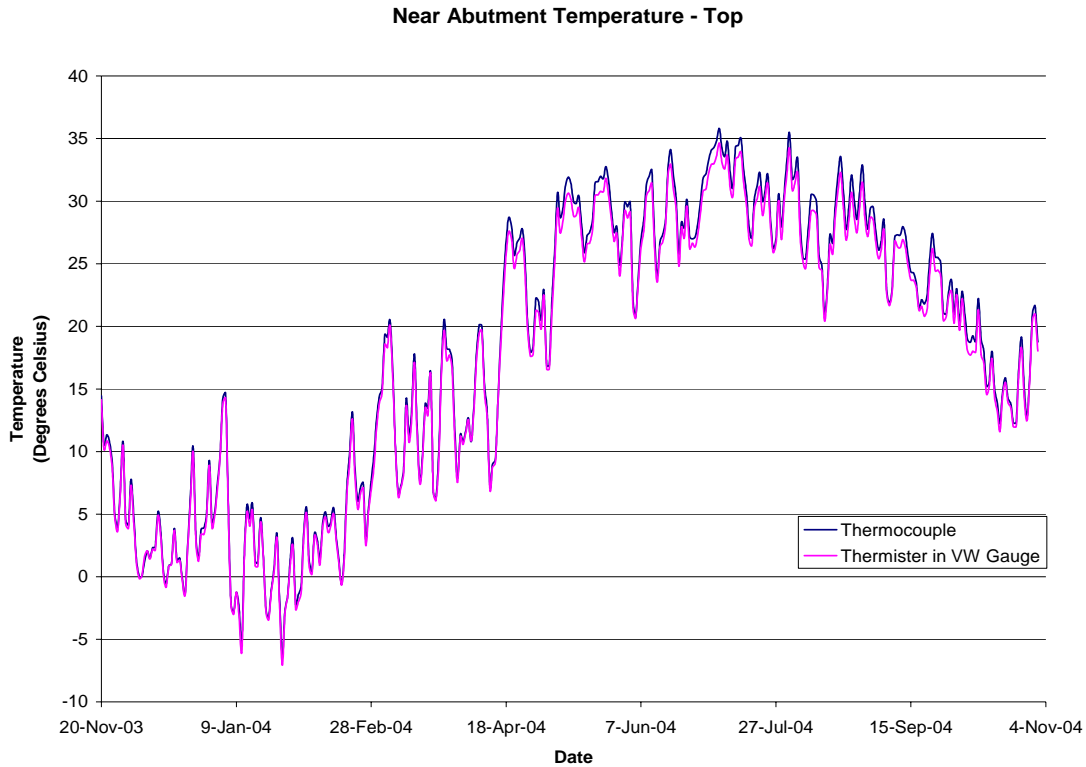
Near Abutment Temperature - Top

Figure 37. Temperature Comparison of Top of Deck at Abutment

GFRP Reinforcing Bar Strains

The readings of the ER strain gauges and VW gauges were recorded every hour. All of the VW gauges worked well throughout the year. However, not all of the ER gauges continued to perform well and some stopped working completely. The status of the ER strain gauges is shown in Table 11. When the status is listed as not continuous that means that the acquisition system was not getting a reading every hour. At some points the system could read a resistance across the strain gauge, but not every hour. When the status is "not working" it means that no readings could be recorded by the data acquisition system. The gauges that had problems are in bold print for easier identification. The "N" represents that the given gauge never had the status. For reference, the live load testing was performed on the bridge on day 209.

Table 11. ER Strain Gauge Statuses

	Beginning Day of Status	
	Not continuous	Not working
ATME1	**247**	N
ATME3	**150**	N
ATME4	N	N
ATME5	N	N
ATME6	**167**	**344**
ATME7	N	N
ATME8	N	N
ATMI1	N	N
ATMI3	N	N
ATMI6	**79**	N
ATMI7	N	N
ATA2	**29**	N
ATA4	N	N
ATA6	**93**	**166**
AL1	N	N
AL2	N	N
AL3	N	N

Both of the original data sets recorded for the ER strain gauges and VW gauges had to be adjusted to get the true change in strain. For the ER strain gauges, the readings recorded were voltages that needed to be converted to strain. This voltage was used in the following equation to calculate the corresponding strain:

$$\Delta \varepsilon = \frac{\dfrac{4000 \times zeroedvoltage}{GF}}{1 - 2(zeroedvoltage/1000)} \tag{9}$$

where $\Delta \varepsilon$ is the change in strain in the GFRP bar measured in microstrain, *zeroedvoltage* is the reading minus the initial reading, and *GF* is the gauge factor, which in this case is 2.1. Due to a difference in sign convention, the signs of the original recorded voltages were reversed before applying Equation 9.

The VW gauges needed to be corrected for temperature fluctuations. A VW gauge reads strain by plucking a tiny wire in the gauge and recording the wire's frequency. Changes in temperature can cause the wire to slacken or tighten which can result in inaccurate strain readings. To account for this, the original reading was adjusted with the following equation:

$$\Delta \varepsilon = (R_1 - R_0)B + (T_1 - T_0)(C_1 - C_2) \tag{10}$$

where R_1 is the recorded strain, R_0 is the initial recorded strain, B is the average batch calibration factor indicated on the VW strain gauge calibration report that comes with the gauges (in this

case B=0.9668), T_1 is the recorded temperature, T_0 is the initial recorded temperature, C_1 is the coefficient of expansion of steel (12.2 $\mu\varepsilon/°C$), and C_2 is the coefficient of expansion of concrete (an average of 10.4 $\mu\varepsilon/°C$).

Figure 38 through Figure 41 show the strains recorded by each group of ER strain gauges, ATME, ATMI, ATA, and AL. For comparison, the corresponding VW strain is included in the plots where applicable.
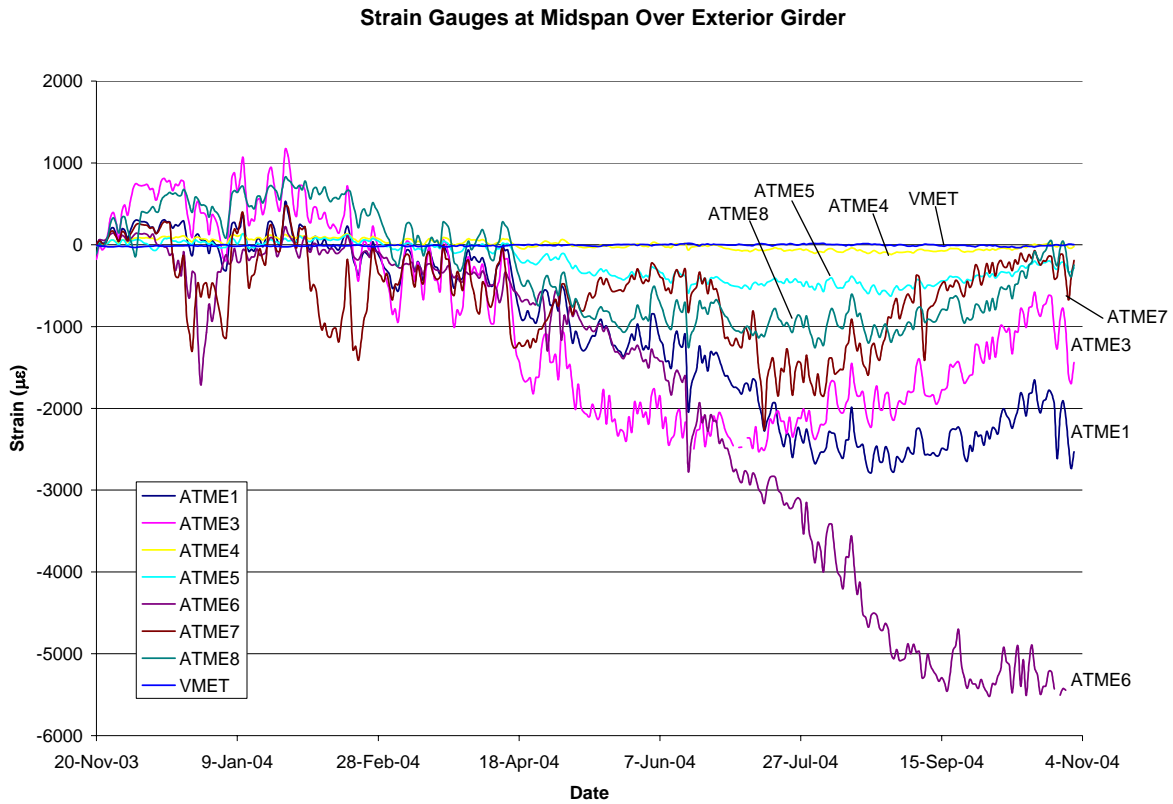
Strain Gauges at Midspan Over Exterior Girder

Figure 38. Transverse Strain Gauges at Midspan over Exterior Girder

Strain Gauges at Midspan Over Interior Girder

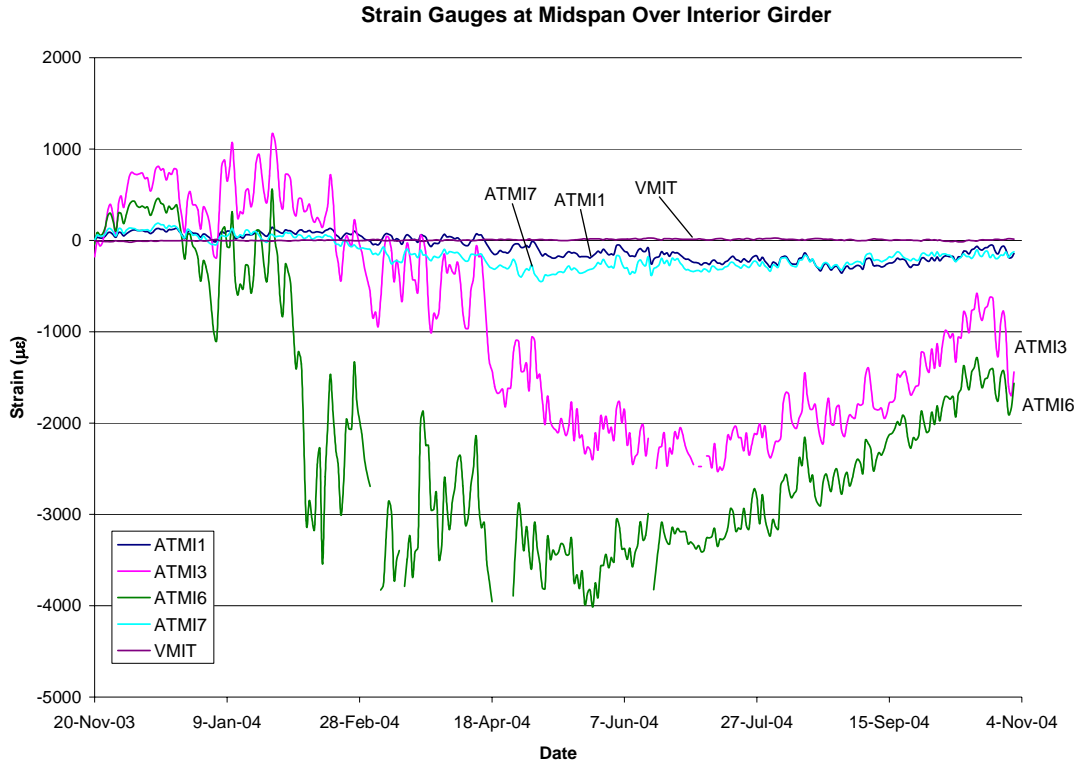**Figure 39. Transverse Strain Gauges at Midspan over Interior Girder**

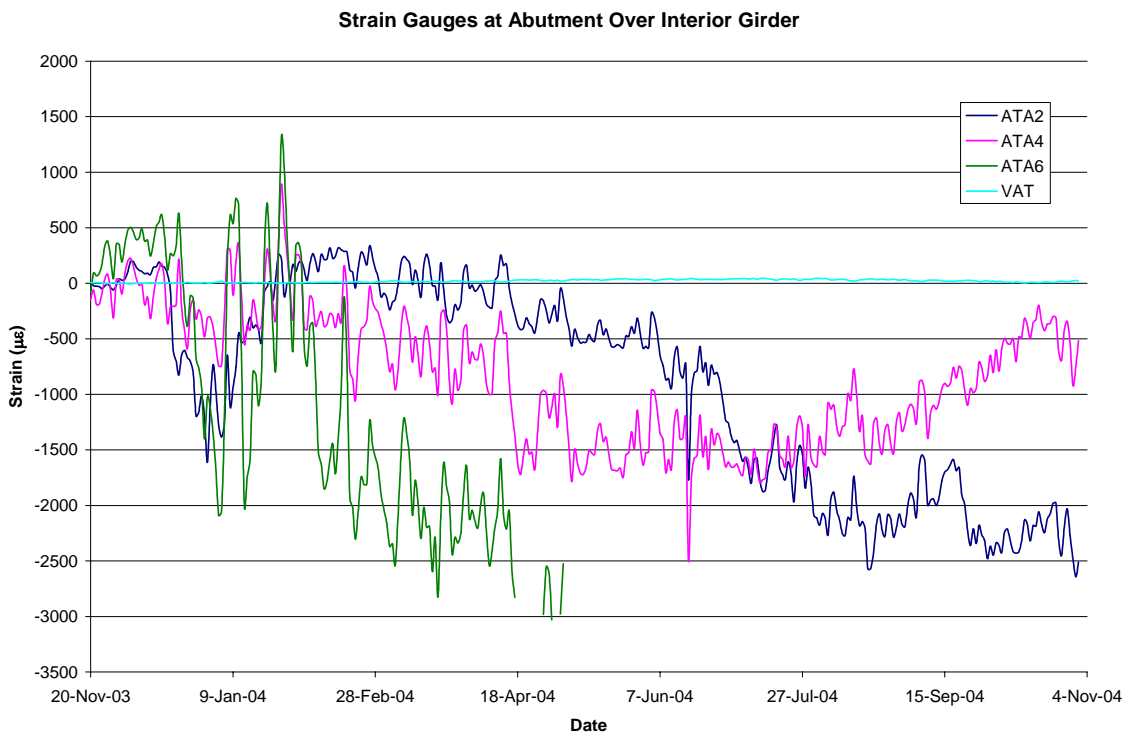**Strain Gauges at Abutment Over Interior Girder**

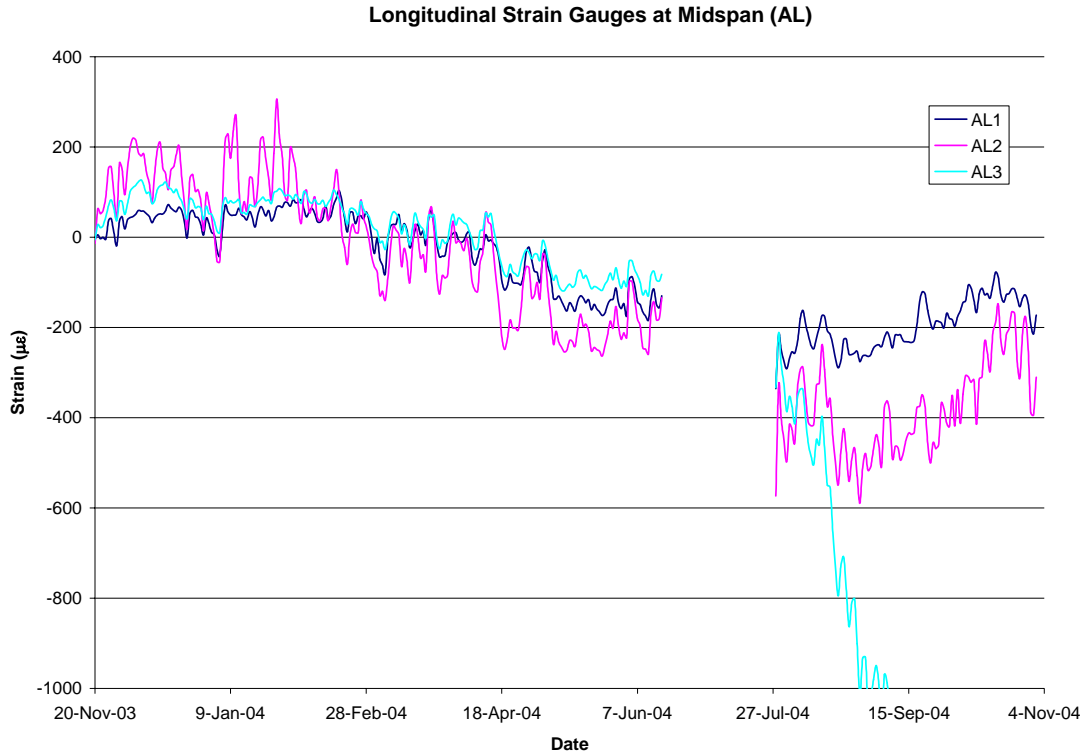**Figure 40. Transverse Strain Gauges at Abutment over Interior Girder**

Figure 41. Longitudinal Strain Gauges at Midspan

The strains measured by the VW gauges were much smaller than the ER strains. Many of the ER strains increased by large proportions as the year progressed. There was drift in some of the gauges causing them to slowly have increasingly higher readings. Any breaks in the data represent a day where the gauge provided no readings due to an error or malfunction in the gauge. An exception was the breaks in the AL readings in Figure 41 they were due to an error in rewiring after the live load testing in June. All of the transverse gauges followed a similar pattern of an increase in compression for the first 100 to 150 days, and then tension for the rest of the year. The ATME gauges followed a similar trend, but many of them started to drift in the later months, especially ATME6. Of the gauges in that group, ATME4 returned the most reasonable results. ATMI3 and ATMI6 followed a similar trend but had very high strains. ATMI1 and ATMI7 had the most reasonable results of the ER strain gauges at the midspan over girder 4. All of the ER strain gauges at the abutment indicated high strains. ATA6 stopped working completely after drifting to about 3000 $\mu\varepsilon$. The longitudinal gauges at midspan had strains that were a little more reasonable but still seemed higher than expected. AL3 had strain readings that increased in tension at a rapid rate, most likely due to drift in the gauge.

In order to find the strain from the VW gauges adjusted for temperature, Equation 10 was applied to the readings recorded in the field. However, the coefficient of thermal expansion of the concrete bridge deck, C_2, was unknown. An average value for concrete was noted previously, 10.4 $\mu\varepsilon$/°C. Depending on the type of coarse aggregate in the concrete mix, the coefficient can vary greatly. In Table 1.3.1 of the *PCI Design Handbook* (1999), the values for concrete with limestone aggregate range from 3.4 to 5.1 $\mu\varepsilon$/°F (6.1 to 9.2 $\mu\varepsilon$/°C). For concrete with quartz sands and gravels as aggregate, the coefficient ranges from 6.0 to 8.7 $\mu\varepsilon$/°F (10.8 to

48

15.7 $\mu\varepsilon/°C$). This large variation in the C_2 value can drastically change the resulting calculated strains. The adjusted strain using different C_2 values for the VW gauge located at the top of the deck at the abutment is illustrated in Figure 42.
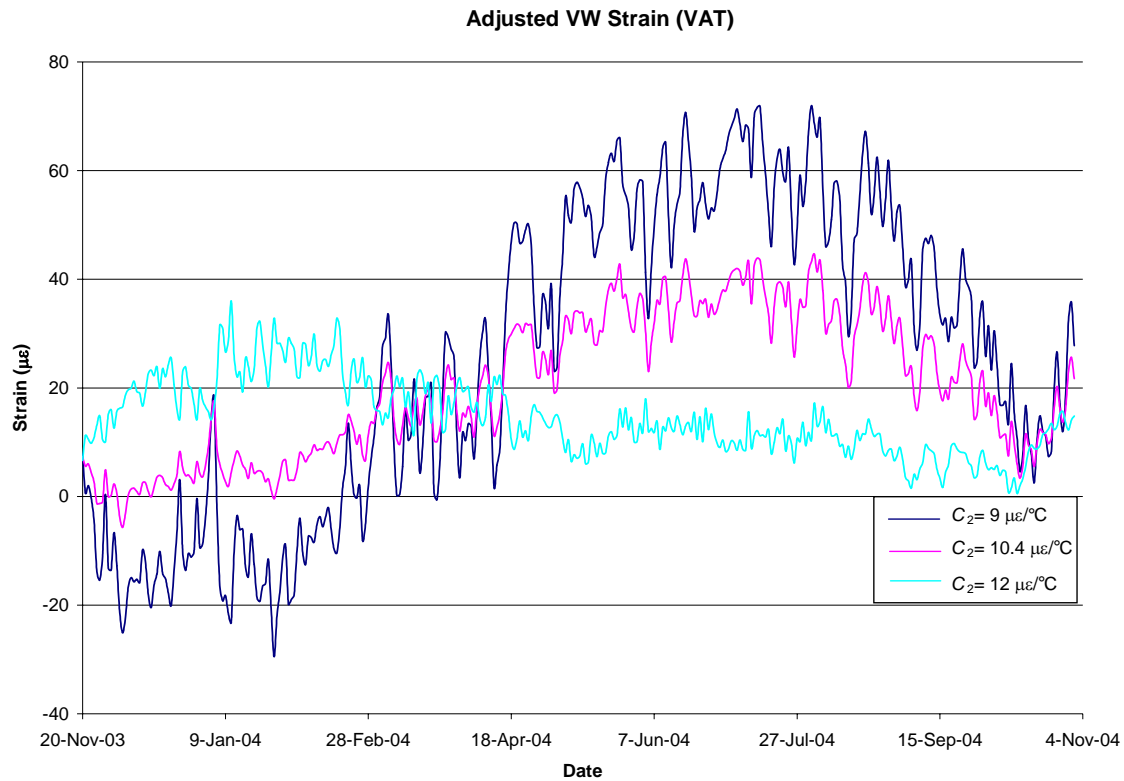
Adjusted VW Strain (VAT)

Figure 42. VW Gauge Strain for Varying Concrete Thermal Coefficients

Figure 42 shows that with smaller C_2 values, the adjusted strains increase. This is because the difference between the coefficient of the vibrating wire in the gauge and the concrete coefficient is increasing. If the C_2 value exceeds the C_1 value, the general trend of tension and compression is reversed. Since the thermal coefficient is unknown, the average value of 10.4 $\mu\varepsilon/°C$ is used for the calculations in this thesis.

Figure 43 and Figure 44 show the strain readings of the VW gauges for the year. Since the strains are only relative to the initial strain, a positive strain may not mean the concrete is in tension since the actual initial strain is unknown. However, the increase or decrease in strain can be observed. All of the VW gauges show a similar trend of slowly increasing in tension and around the end of July becoming more compressive. The strains at the abutment followed the same pattern of changes and were about 30 $\mu\varepsilon$ apart in the beginning of testing and the difference slowly increased to about 50 $\mu\varepsilon$. For the gauges over girder 4, the top of the deck experienced a slightly greater increase in strain at the abutment than at the midspan. The reverse was true for the bottom of the deck, with the midspan having a greater change in strain than at the abutment. The bottom of the deck at the same location was mostly in compression. The bottom of the deck at midspan over girder 5 followed the same pattern as the bottom at girder 4 except it did not experience as much compression. It would make sense that less compression was experienced by the gauges at girder 5 since there is less restraint at the exterior girder than at the interior

49

girder. The top of the deck at the midspan over the interior and exterior girders experienced the same strain changes. Again, please note the magnitudes and even the trends of tension and compression could be different if the actual concrete coefficient of thermal expansion is different than the 10.4 με/°C used.

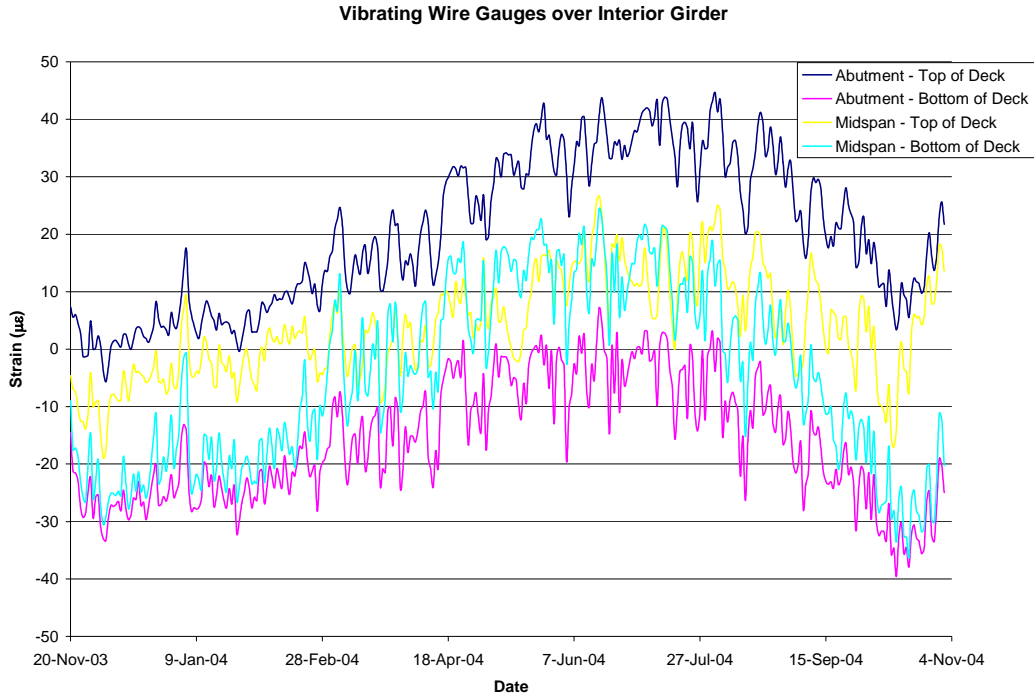**Vibrating Wire Gauges over Interior Girder**

Figure 43. VW Gauges over Interior Girder

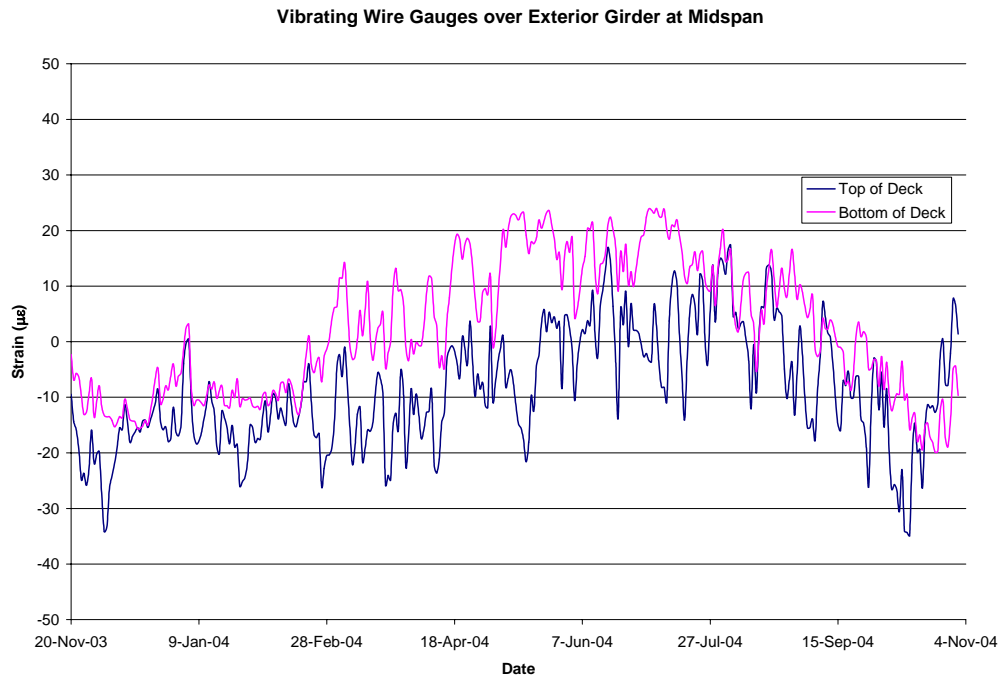**Vibrating Wire Gauges over Exterior Girder at Midspan**

Figure 44. VW Gauges over Exterior Girder

50

Over the year, the strains measured by the VW gauges fluctuated. Table 12 shows the difference between the maximum and minimum strains experienced through the year of testing. The table includes the differences from both the raw data and from the average daily data. The strain differences show that at the gauged locations over the interior girder, the bottom of the deck experienced more change in strain than the top. However, at midspan over the exterior girder, the top of the deck experienced more change in strain than the bottom. Comparing the two data sets used for determining the differences in strain demonstrates how averaging data can at times skew the results. With the strains of each day averaged to one point, the variation of the strain was decreased.

Table 12. Yearly VW Gauge Strain Differences ($\mu\varepsilon$)

	Abutment Interior		Midspan Interior		Midspan Exterior	
	Top	Bottom	Top	Bottom	Top	Bottom
Raw Data	74	91	65	105	88	73
Daily Average	50	47	46	61	52	44

Figure 45 compares the strain changes recorded by the ER strain gauge and the VW gauges. ATME4 was used for this comparison since it was the gauge with the least amount of strain variation, and, therefore, the most accurate of the ER strain gauges. The graph shows the hourly strain readings for two 5-day periods taken out of the year of monitoring. The two weeks shown are the first week and then a week about 100 days before the end of the monitoring. Daily fluctuation in strain occurs mainly from temperature changes. During both weeks, the VW gauges varied about 25 $\mu\varepsilon$. The ER strain gauge varied about 100 $\mu\varepsilon$. However, over the months in between the strain had shifted down approximately 100 $\mu\varepsilon$. The ER strain gauge and the VW gauge have opposite trends. When the strain from the ER gauge is decreasing, the VW gauge is showing an increase or more tensile strain. This could indicate that the assumed concrete thermal coefficient was too low. If the coefficient were higher, the two gauges would follow the same trend.

Figure 46 shows a worst case of how the ER strain gauges were not as reliable as VW gauges. This ER gauge went from fluctuating about 250 $\mu\varepsilon$ in a day to 1500 $\mu\varepsilon$. It also shifted about 1500 $\mu\varepsilon$. The breaks in the later readings of the ATA2 gauge were when the gauge was not operating correctly and did not provide a reading. Again, the VW gauge was much more consistent, yet followed an opposite pattern of fluctuating strain.

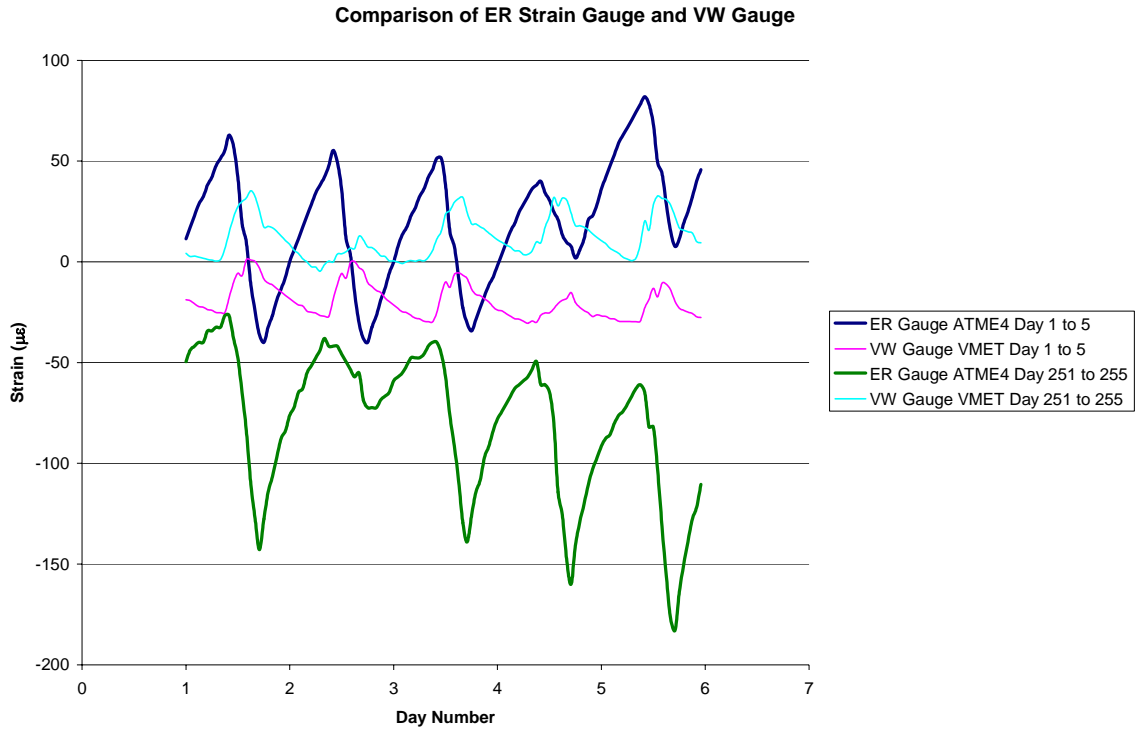**Comparison of ER Strain Gauge and VW Gauge**

Figure 45. Daily Comparison of ER Strain Gauge and VW Gauge at Midspan

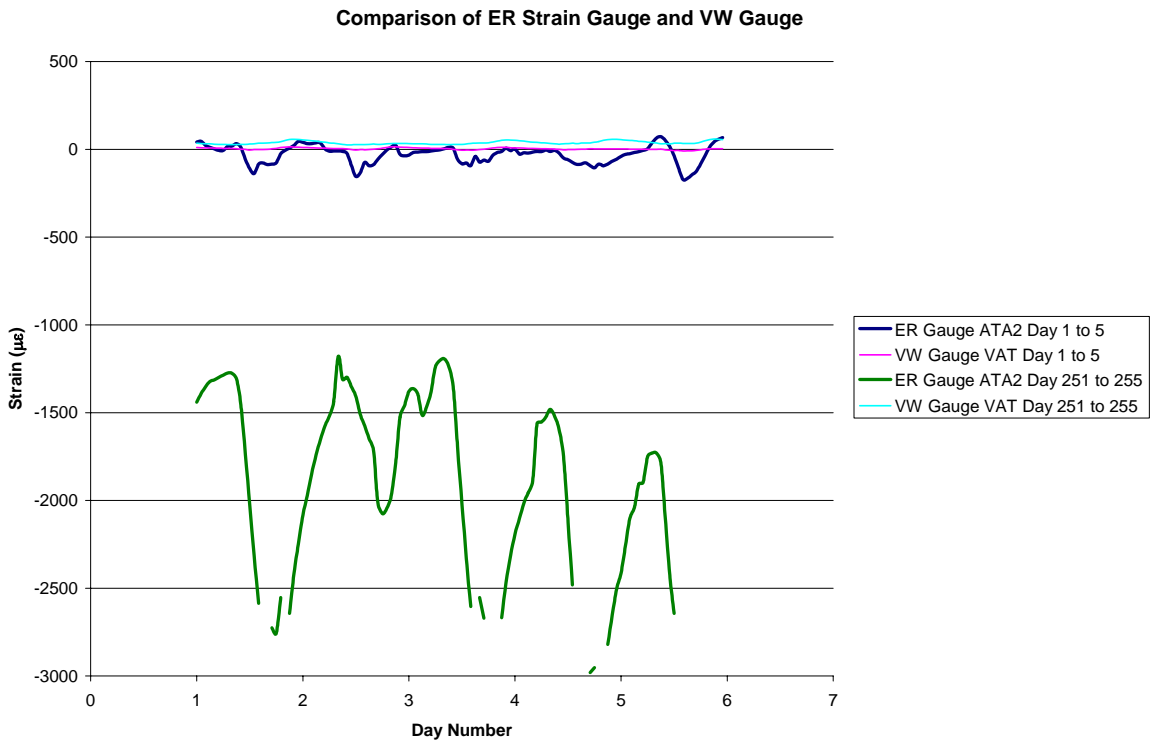**Comparison of ER Strain Gauge and VW Gauge**

Figure 46. Daily Comparison of ER Strain Gauge and VW Gauge at Abutment

52

By comparing the results of the ER strain gauges and the VW gauges, it can be concluded that the ER strain gauges lose accuracy rapidly over time and should not be used for long-term monitoring of a bridge deck. However, the ER gauges may be useful in determining general trends in the strain changes but not necessarily the magnitude of those changes. To get a better idea of the pattern that the ER gauges and VW gauges followed for the year of monitoring, Figure 47 compares two gauges at the same location. Notice that the ER strain gauges and VW gauges are plotted on a different scale to better compare the general strain changes.
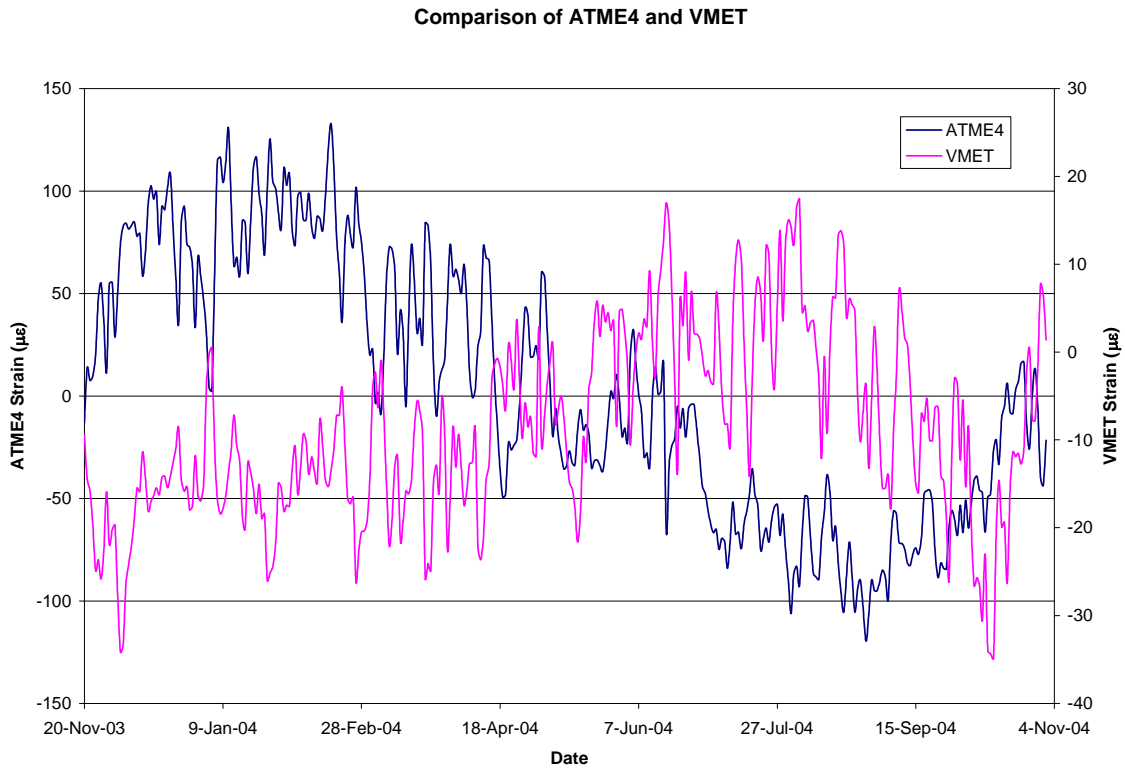
Comparison of ATME4 and VMET

Figure 47. Comparison of ATME4 and VMET

Relationship Between Temperature and Strain

From the plots of the daily fluctuations of strain, it appears that temperature plays a role in affecting the strain in the GFRP reinforcing bars and in the concrete. Figure 48 shows the relationship between the thermister temperature and ER strain at midspan over the exterior girder. Figure 49 shows how the VW strain compares to the temperature at the same location. The ER strain is inversely proportional to the temperature. Therefore, when the temperature increases the strain becomes more compressive. This trend makes sense if the deck is restrained from movement. As the temperature rises, the deck wants to expand. If the deck is restrained, it cannot expand creating compressive stresses in the deck. The VW gauges show that the strain increases with increased temperature. The deck would expand with the temperature rises if it were unrestrained, but the VW gauge would not indicate that increased tension since the readings are adjusted for thermal expansion. There must be an error in the concrete thermal coefficient used to calculate the adjusted strain or an error in the VW gauge itself or its installation.

ATME4 and Temperature
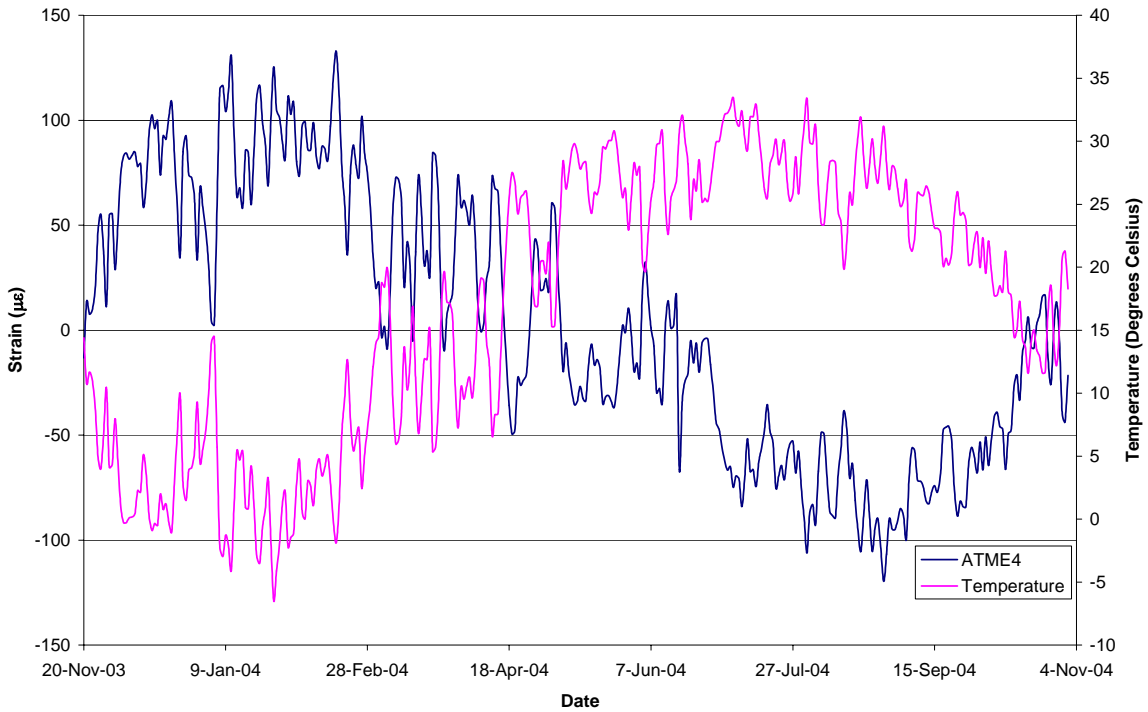
Figure 48. Comparison of ER Strain and Temperature

VMET and Temperature
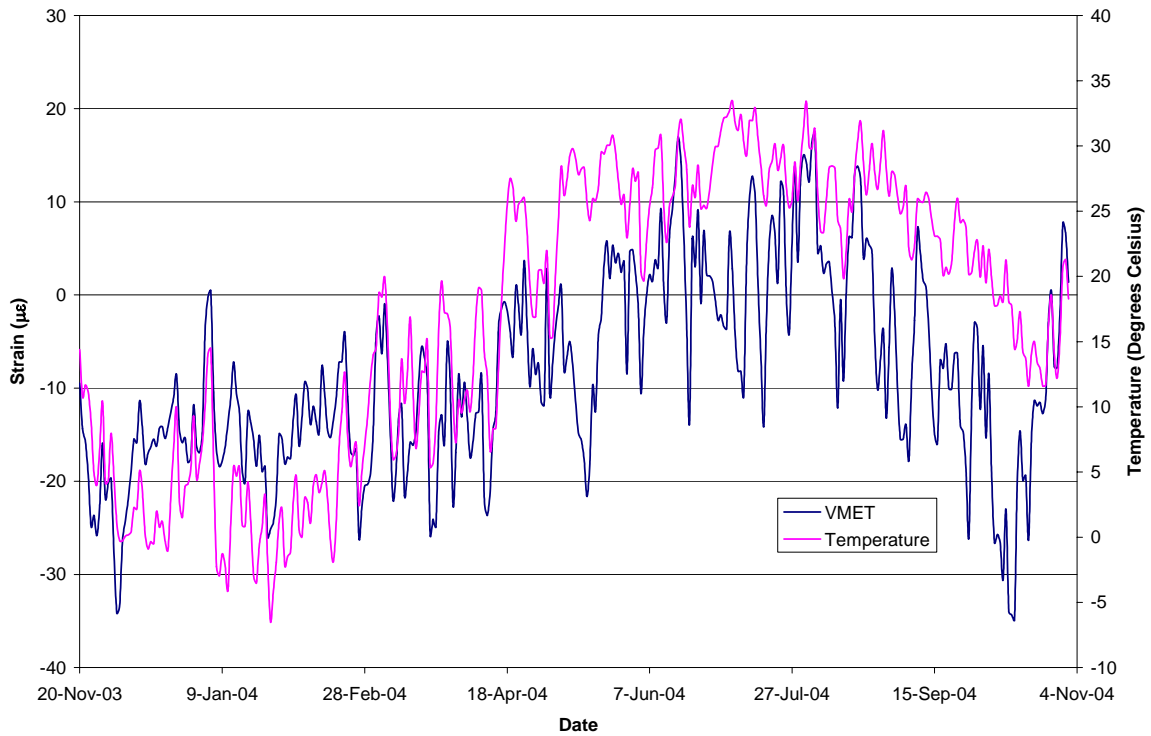
Figure 49. Comparison of VW Strain and Temperature

Figure 50 shows that the VW strain changes lagged behind the temperature changes. This means that after the temperature had reached its lowest point and was starting to increase, the VW gauge strains were still decreasing. The ER gauges lined up with the temperature better than the VW as shown in Figure 51. Note that the strain axis for the ER gauge has been reversed for a better comparison.
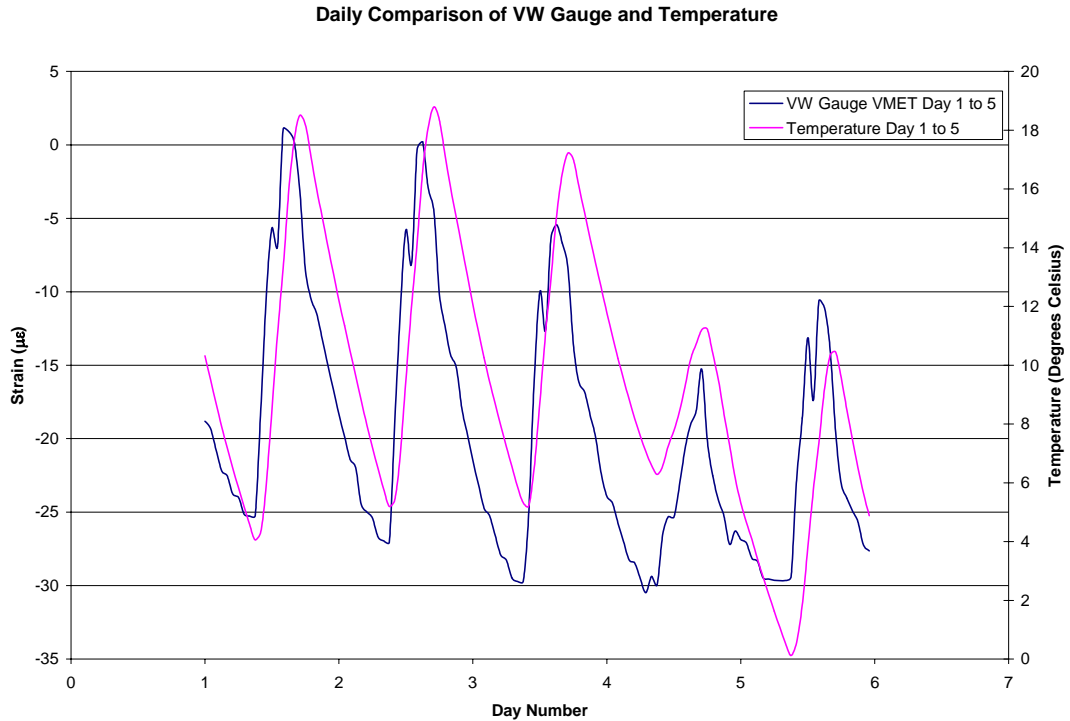
Figure 50. Daily Comparison of VW Gauge Strain and Temperature

Figure 51. Daily Comparison of ER Gauge Strain and Temperature

55

The main reason for monitoring the strains in the bridge deck for a year was to determine if the strains in the concrete are consistent, perhaps indicating if the GFRP is performing adequately. To determine this, two days with similar average temperatures were chosen and their corresponding average strains were compared. Table 13 and Table 15 show two samples of the long-term strain changes in the VW gauges, and Table 14 and Table 16 show the changes in the ER gauges. In Table 13 and Table 14 there were 184 days between the two dates. Table 15 and Table 16 had 237 days between the two dates.

Table 13. Comparison of VW Gauge Strains after 184 Days

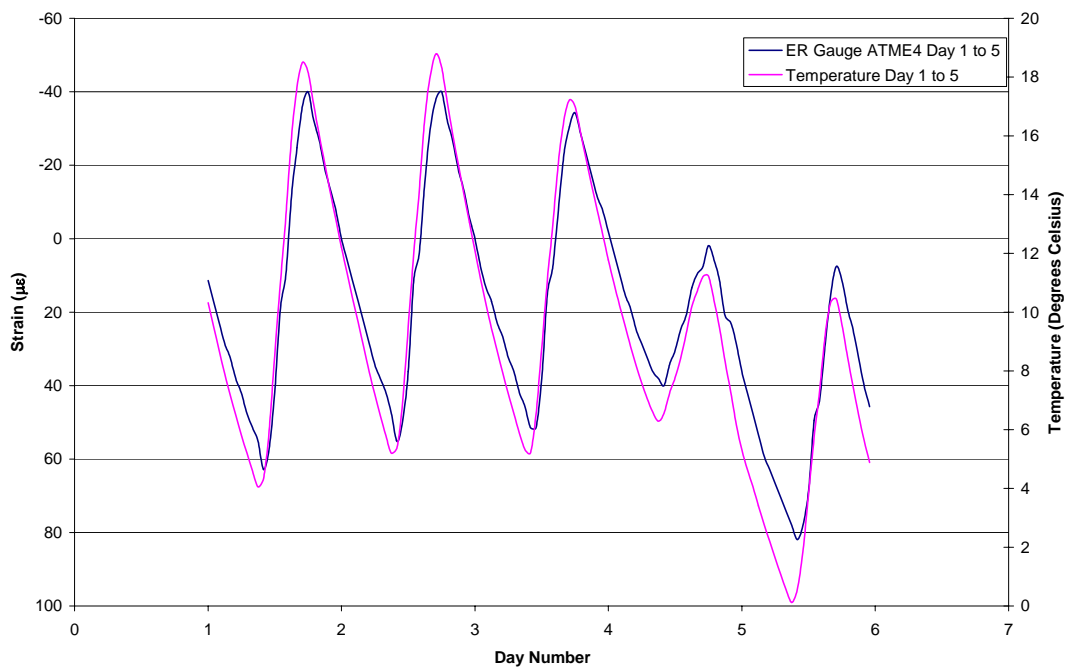| | | 30-Apr-04 | | 31-Oct-04 | | |
		Avg. Temp °C	Avg. Strain με	Avg. Temp °C	Avg. Strain με	.Δε με
VW Strain Gauge	VAT	21.1	25.4	21.0	25.6	**0.3**
	VAB	20.4	-11.6	20.6	-20.2	**-8.6**
	VMIT	21.5	3.2	21.4	17.6	**14.4**
	VMIB	20.8	5.3	21.0	-12.3	**-17.6**
	VMET	20.5	-11.5	21.3	6.6	**18.1**
	VMEB	20.1	9.5	21.1	-4.4	**-13.9**

Table 14. Comparison of ER Gauge Strains after 184 Days

| | | 30-Apr-04 | | 31-Oct-04 | | |
		Avg. Temp °C	Avg. Strain με	Avg. Temp °C	Avg. Strain με	.Δε με
ER Strain Gauge	ATA2	21.1	-282	21.0	-2642	**-2360**
	ATA4		-1117		-745	**372**
	ATA6		-3030		-	**N/A**
	ATMI1	21.5	-76	21.4	-187	**-112**
	ATMI3		-533		-751	**-218**
	ATMI6		-3398		-1827	**1571**
	ATMI7		-353		-144	**208**
	ATME1	20.5	-731	21.3	-2734	**-2003**
	ATME3		-1434		-1698	**-264**
	ATME4		19		-44	**-63**
	ATME5		-177		-327	**-150**
	ATME6		-743		-	**N/A**
	ATME7		-734		-404	**329**
	ATME8		-517		-390	**127**

Table 15. Comparison of VW Gauge Strains after 237 Days

		1-Mar-04		24-Oct-04		
		Avg. Temp °C	Avg. Strain με	Avg. Temp °C	Avg. Strain με	Δε με
VW Strain Gauge	VAT	11.8	13.5	12.0	10.7	**-2.8**
	VAB	11.3	-17.4	11.9	-34.6	**-17.3**
	VMIT	12.7	-3.0	12.0	5.5	**8.6**
	VMIB	12.2	-4.2	11.7	-31.0	**-26.8**
	VMET	12.1	-19.2	11.7	-11.2	**8.0**
	VMEB	11.8	3.9	11.6	-19.7	**-23.6**

Table 16. Comparison of ER Gauge Strains after 237 Days

		1-Mar-04		24-Oct-04		
		Avg. Temp °C	Avg. Strain με	Avg. Temp °C	Avg. Strain με	Δε με
ER Strain Gauge	ATA2	11.8	-122	12.0	-1978	**-1856**
	ATA4		-365		-310	**55**
	ATA6		-1897		-	**N/A**
	ATMI1	12.7	14	12.0	-56	**-70**
	ATMI3		-175		-532	**-357**
	ATMI6		-2417		-1410	**1007**
	ATMI7		-89		-155	**-65**
	ATME1	12.1	-269	11.7	-1819	**-1549**
	ATME3		-314		-636	**-323**
	ATME4		35		17	**-18**
	ATME5		-7		-214	**-208**
	ATME6		-165		-5221	**-5056**
	ATME7		-454		-147	**306**
	ATME8		202		47	**-155**

The VW gauges had much more consistent results than the ER gauges. The VW gauges located in the bottom of the deck all became more compressive over time. The VW gauged near the top of the deck mostly became more tensile over time. The strain differences over time were less for the VW gauges than for the ER gauges but were significant when compared to the strain changes over the year of monitoring. For example, the gauge VMIB had a strain reading difference of 26.8 με, but the strain only varied 61 με over the year. The ER gauges had larger strain differences and the changes were not consistent within each group. In addition, for the ER gauges, the larger time period between the compared readings did not always result in a larger difference in strain. The sampling used may not be completely representative of each case, especially since each day's temperatures and strains were averaged. However, it does indicate that the ER gauges are not reliable in their results and that the VW gauges' strains have increased over the year of monitoring.

CONCLUSIONS

Conclusions from Construction Monitoring

The construction of the Gills Creek Bridge, and more specifically the bridge deck, was monitored to determine the constructibility of bridge decks reinforced with GFRP. The same crew installed the bars in both Spans A and C, and the installation of the Span A GFRP bars took about a half day longer than the Span C steel bars. Installation of Span A reinforcement lasted about a full day, while the installation of Span C reinforcement last about a half day. The time it took for the crew to install the top mat GFRP bars in Span A was about the same as it took for them to install both mats of steel bars in Span C. It was clear that the crew was very experienced in installing epoxy-coated steel bars. In Span C, both mats were installed with little or no conversation amongst the crew. The bars were handled, installed, and tied with a minimal amount of delays or questions. Conversely, the crew was clearly inexperienced in handling the GFRP bars. However, after an hour or two its production was just as swift as with the steel bars. The major factor in the increased amount of installation time for the GFRP bars was the fact that there was almost two times the number of bars as in Span C. Moreover, the bars were spaced very closely, so more ties were necessary and due to the tight spaces, it was more difficult to install the ties. Some comments on the installation of the GFRP bars from the crew were as follows:

- the rough, sand-impregnated surface of the bars required gloves to be worn at all times,
- the lightweight nature of the bars made it much easier to carry a bundle of bars and lay them in their approximate locations,
- the increased flexibility of the bars was a concern, but chairs were spaced at closer intervals than in Span C to alleviate that, requiring more time to install the bars,
- the increased number of ties was the biggest complaint, due to the increased number of bars and the necessity of tying the top mat to the bottom mat to prevent floatation of the bars during concrete casting.

Overall, the installation of the GFRP bars went smoothly when compared to that of the steel bars. The increased installation time for the GFRP bars was mainly due to the increased number of bars in Span A. The workers were unfamiliar with the material at first, but by the end of the day were handling, installing, and tying the GFRP bars with skill. From the monitoring of the construction of the Route 668 bridge over Gills Creek, it can be concluded that GFRP bars are an acceptable material in bridge deck applications with respect to constructibility issues.

Conclusions from Live Load Testing

The live load testing of the Gills Creek Bridge provided valuable insight on the change in strain of GFRP bars and how the changes affect factors of design such as girder distribution factors and dynamic load allowances.

Strains and Stresses in the GFRP Reinforcement

The stresses calculated from the quasi-static and dynamic tests all showed that the transverse GFRP bars were experiencing more compression during the 2004 live load test than during the initial test. The highest tensile stresses occurred at the interior girder at the abutment during the dynamic test. The transverse bars experienced a tensile stress of 75 psi. This is well below the ACI 440 specified allowable tensile stress of 13.9 ksi and far less than the bar's measured tensile strength in the lab of 109 ksi. The largest compressive stress of -130 psi occurred at the interior girder at midspan during the dynamic test. ACI 440 does not specify an allowable compressive stress for FRP because creep rupture is not a problem in compression. The stress recorded in this case is so small that it can be assumed that the concrete can carry the stress. In all instrumented groups of reinforcing bars, the strains in the groups were relatively uniform at the instant one of the gauges registered a peak strain.

From the stresses calculated, it can be concluded that the top mat of transverse GFRP reinforcement is designed conservatively, however it should be noted that no cracks could be found in the bridge deck upon visual inspection. It is impossible to tell if the bars stresses would still fall below the allowable stresses if the bridge deck were cracked.

No comparisons could be made between Span A and Span C since not enough of the ER strain gauges were operable in Span C.

Girder Distribution Factors

The girder responses measured using the deflectometers, ER strain gauges, and WIM gauges showed that Span A had greater deflections and girder strains for both the quasi-static and dynamic tests. The largest responses resulted from the dynamic tests. The greatest deflection was 0.11 in in Span A. The maximum ER strain and WIM strain were 145 $\mu\varepsilon$ and 104 $\mu\varepsilon$, respectively. The ER strain gauges and WIM gauges followed the same pattern, but for all causes the strain readings of the WIM gauges were lower than the ER strain gauges. In Span A, the highest responses were in the girder closest to the truck orientation.

The girder distribution factors calculated from the 2004 live load testing were not significantly different from the initial testing. There was no clear trend of an increase or decrease in GDF values between the two test dates. For the interior truck orientation, the different methods used to calculate the GDF values resulted in conflicting trends of increasing or decreasing since 2003. In Span A, the largest factor was S/10.0 measured by the ER strain gauges in 2004. In Span C, the largest factor was S/9.7 measured by the WIM gauges in 2004. Both of these values are well below the limits specified by the AASHTO Standard Specification and the AASHTO LRFD Specification of S/7.0 and S/7.4, respectively. For the exterior orientation, the 2004 Span A results were slightly lower than in 2003, and the Span C results indicated a slight increase in the distribution factors. In Span A, the largest factor was S/8.0 measured by the ER strain gauges in 2003. Span C had a maximum factor of S/8.1 measured by the WIM gauges in 2004. Again, these values were less than the AASHTO Standard and AASHTO LRFD design limit of S/6.5 calculated using the lever rule. From these comparisons, it can be concluded that the bridge was designed conservatively with respect to transverse load

distribution and that no significant changes in the distribution of load were seen after 1 year of service.

When comparing the distribution factors for Span A and Span C, the two spans distribute the load similarly. In 2004 for the interior truck orientation, the values calculated for Span A ranged from S/10.0 to S/11.2. For Span C, the distribution factors were from S/9.7 to S/12.3. For the exterior truck orientation, the values for Span A ranged from S/8.3 to S/9.6 and for Span C were between S/8.1 to S/8.6. These differences are minimal. Therefore, it can be concluded that the span reinforced with GFRP bars is distributing the transverse load the same as the span reinforced with epoxy-coated steel bars. Note that the deck was uncracked at the time of both live load tests, and that cracking could cause the loads to be distributed differently.

Dynamic Load Allowance

The dynamic load allowance results show that the impact factors increased between 2003 and 2004. Using the deflection data for Span A, the impact factors increased from 0.36 to 0.52 when traveling northbound, and from 0.18 to 0.37 when traveling southbound. For Span C, the northbound values increased from 0.11 to 0.36. However, the southbound values decreased from 0.22 to 0.18. Many of the 2004 values were above the AASHTO Standard Specification design value of 0.29 and the AASHTO LRFD Specification design value of 0.33. Using the ER strain data, similar trends were seen, but the impact factors were smaller. For Span A, the live load tests carried out in 2003 resulted in negative values of -0.84 traveling northbound and -0.87 traveling southbound. These were erroneous results from malfunctioned gauges, so they cannot be compared to the 2004 values. In 2004, Span A had impact factors of 0.53 traveling northbound and 0.31 traveling southbound. For Span C, the northbound value increased from 0.06 to 0.12 and the southbound value decreased from 0.23 to 0.22. The Span A results were higher than the AASHTO design values. The WIM gauges were only installed in the 2004 testing. The impact factors calculated using their data was at Span A traveling northbound, 0.62, and southbound, 0.34. At Span C, the values were 0.13 traveling northbound and 0.23 traveling southbound.

The increase in impact factors over just 1 year is a cause for some concern. Dynamic load allowances can be increased by a change in the riding-surface roughness, profile differences in the approaches, or a difference in the suspension of trucks. However, no significant changes in the roadway or approaches were seen upon visual inspection and the same truck was used for both live load sessions. Although the impact factors were above the design values, there was no cracking or unusual behavior of the structure seen during testing. The highest stress seen in the girders was 4.62 ksi, less than 10% of the tensile strength of the girders. Additional live load tests must be performed to see if the impact factors continue to increase and to determine if the GFRP-reinforcement is playing a role in the increase.

Comparison of Electrical Resistance Strain Gauges and Weigh-in-motion Strain Gauges

In both tests, the WIM gauges had similar strain readings to the ER strain gauges at the girders further from the load. However, in the girders closest to the load, the strains from the WIM gauges were much less than those from the ER gauges. The same types of differences

were seen in both the quasi-static and dynamic tests from both dates of testing. It can be concluded that WIM gauges are not adequate to record accurate strains in place of ER strain gauges. Future tests using WIM gauges and ER strain gauges in tandem may allow researchers to calibrate the WIM gauges to produce similar results to the ER strain gauges.

Long-Term Monitoring Conclusions

Temperatures

The temperatures in the bridge's concrete deck were taken by thermocouples and thermisters within the VW gauges. Both the thermocouples and the thermisters reported very similar temperatures. As expected the temperatures at the top of the deck typically were a little higher than at the bottom. At the locations where the middle temperature was recorded, the middle temperature was always in-between the top and bottom temperatures. By comparing the two sources of temperature data, it can be concluded that the instrumentation is recording an accurate deck temperature.

GFRP Reinforcing Bar Strains

The GFRP reinforcing bars strains were measured by ER strain gauges and VW gauges. Of the original 27 ER gauges, 17 of them were operable at the time of installation of the long-term data acquisition system. Over 1 year of testing, six gauges had times during which they did not take readings due to a malfunction in the gauge. Two of those six gauges stopped working completely by the end of the year. From this, ER gauges showed that they do not have a long lifespan when used in the field. Additionally, the ER gauges were installed in four groups. Aside from the AL group with a gauge over girders 1, 3, and 5, the gauges within each group were relatively close together. The ER gauges within each group did not have similar readings as expected. Many of the strains reported by the gauges appeared to drift, often into the thousands of microstrain. Due to the inconsistency of the readings and the frequency that the ER strain gauges were becoming inoperable, it was concluded that the data from the ER strain gauges could not be used alone in determining the long-term health of the GFRP reinforcing bars and bridge deck. They could, however, be useful in determining trends in the strain changes.

The VW gauges reported much smaller and consistent strains than the ER gauges. Over the year, the greatest variation in the VW strain gauge readings was 107 $\mu\varepsilon$ at the midspan over girder 4. This variation was much lower than that of the ER strain gauges. Since the concrete coefficient of thermal expansion was not measured for the deck, the VW gauges results were not as reliable as expected. For the continued long-term monitoring performed on the Gills Creek Bridge, only the strains from the VW gauges should be considered along with the trends shown by the operable ER gauges.

Relationship Between Temperature and Strain

The strains in the bridge deck were directly proportional to the change in temperature according to the VW gauges. As the temperature increased, the strains in the deck became more tensile. The ER gauges indicated the opposite, that the strains are inversely proportional to

temperature. The use of a different concrete thermal coefficient may indicate that the VW gauges are reading strains following a similar pattern as the ER gauges. Both gauges followed the temperature changes closely showing that temperature is primary controlling factor of the strains in concrete and in the GFRP reinforcement bars when the bridge deck is restrained.

RECOMMENDATIONS

1. In the design of bridge decks reinforced with GFRP as top mat reinforcement, the simplified strip method for deck design recommended by the AASHTO Standard Specifications and the AASHTO LRFD Bridge Design Specifications should be followed.

2. The design of the GFRP reinforcement should conform to the recommendations of the *ACI Guide for the Design and Construction of Concrete Reinforced with FRP Bars (2003)*.

3. Electrical resistance strain gauges should not be used for long-term monitoring of embedded reinforcing bars.

4. To ensure proper interpretation of data from embedded vibrating wire gages, samples of the concrete should be made to evaluate the coefficient of thermal expansion.

5. Weigh-in-motion gauges should be calibrated prior to use in the field, as they typically measured smaller strains than the bonded electrical resistance gauges.

COSTS AND BENEFITS ASSESSMENT

Table 17 presents the material and installed costs for bare steel, epoxy-coated reinforcing steel (ECR), and stainless steel reinforcement (VDOT, 2004; Pianca, F., personal communication, 2005). GFRP is priced by the linear foot, since its density differs significantly from that of steel. Span A contains 7,000 lf of GFRP reinforcing bars and 5,069 lb of ECR. Span C contains 5,676 lb of ECR. The installed cost for Span A can be determined, and the differences in costs versus bare steel, all ECR, and stainless steel, are shown in Table 18.

The price of a concrete overlay, including milling, patching, and traffic control, for a deck that reaches rehabilitation prior to the 75-year design life averaged $12.03 per square foot in 2004. Thus, the additional costs for alternative reinforcements, even for solid stainless steel

Table 17. Reinforcement Costs

Type	Installed Price
Bare	$ 0.424/lb
ECR	$ 0.637/lb
GFRP	$ 0.900/l.f.
Stainless steel	$ 2.360/lb

Table 18. Unit Costs for Deck Reinforcement

	Installed	
Type	Unit Cost ($/ft^2)	Cost Increase Over Bare Steel ($/ft^2)
Bare	$ 1.91	-
ECR	$ 2.65	$ 0.74
GFRP/ECR	$ 6.98	$ 5.07
Stainless Steel	$ 9.81	$ 7.90

reinforcement at $7.90 per square foot more than bare steel and GFRP at $5.07 per square foot more than bare steel, is less than the cost of one concrete overlay, including traffic control costs, before adjusting for inflation. However, the cost differential for GFRP top mat reinforcement, at $4.33 per square foot over that of all ECR, compares favorably when its inherent immunity to conventional corrosion-related damage is considered.

SUGGESTIONS FOR FURTHER RESEARCH

This research is another step toward understanding the performance and durability of GFRP reinforcement bars. The use of GFRP bars in concrete bridge decks is still a new concept. Before GFRP can be accepted as a reliable and cost effective material, more research is required. Some recommendations for future research involving GFRP reinforcement are presented in this section.

The monitoring of the Gills Creek Bridge should be continued. Changes in strain and temperature over the years of service would indicate the performance of the GFRP bars. The performance of the bridge deck when cracking begins to occur should be examined. In addition, with continued monitoring, the durability of the testing instruments can be determined. In future projects, fiber optic sensors should be used to track the change in strain of the GFRP bars since they are more reliable than ER strain gauges. Similar spans reinforced with GFRP and steel should be monitored together to see how the two materials compare. Long-term monitoring of bridges in service is the best way to determine the durability of GFRP bars.

Furthermore, additional live load tests should be completed throughout the bridge's life. After 1 year of service, no cracking was detected. Later live load tests could address the concern with cracking of the deck and the expected increase in flexibility of GFRP. Specifically, the dynamic load allowances should be observed to ensure that the impact factors are not continuing to increase with time.

The validity of the WIM gauges is another issue that should be investigated further. The ease of installation of WIM gauges makes them an attractive replacement for ER strain gauges. However, additional live load tests need to be performed to confirm if they are acceptable for this kind of application.

Future live load tests should also include the use of multiple trucks. With the use of multiple trucks, the girder distribution factors for two or more lanes loaded can be evaluated and compared to the AASHTO design standards.

It is hoped that with future research, the dependability of GFRP bars as reinforcement in concrete bridge decks will be verified leading to an increase in the ease of construction, improvement of the durability of bridge decks, and a reduction in maintenance costs.

REFERENCES

American Association of State Highway and Transportation Officials (1998). *AASHTO LRFD Bridge Design Specifications*, Second Edition, Washington, DC.

American Association of State Highway and Transportation Officials (2002). *AASHTO Standard Specifications for Highway Bridges*, 17th Edition, Washington, DC.

ACI Committee 440 (2003). *ACI Guide for the Design and Construction of Concrete Reinforced with FRP Bars*, ACI 440.1R-03, American Concrete Institute, Farmington Hills, MI.

Bank, L.C., Gentry, T.R., Barkatt, A., Prian, L., Wang, F. and Mangla, S.R. (1998). Accelerated Aging of Pultruded Glass/Vinyl Ester Rods, Fiber Composites in Infrastructure, *Proceedings of the Second International Conference on Fiber Composites in Infrastructure,* ICCI'98, Vol. 2, pp. 423-437.

Benmokrane, B., El-Salakawy, E., Desgagné, G., and Lackey, T. (2004). FRP Bars for Bridges, *Concrete International*, Vol. 26, No. 8, pp. 84-90.

Bhise, Vikrant S. (2002). *Strength Degradation of GFRP Bars*, M.S. Thesis, Virginia Polytechnic Institute and State University, Blacksburg, VA.

Chong, K. (1998). Durability of Composite Materials and Structures, *Durability of Fibre Reinforced Polymer (FRP) Composites for Construction – Proceedings of the first International Conference (CDCC)*, pp. 1-12.

Dejke, V. (2001). *Durability of FRP Reinforcement in Concrete*, Goteborg, Sweden, Reproservice, Chalmers.

Gentry, T., Bank, L., Thompson, B., and Russell, J.(2002). An Accelerated-test-based Specification for Fiber Reinforced Plastics for Structural Systems, *Durability of Fibre Reinforced Polymer (FRP) Composites for Construction – Proceedings of the second International Conference (CDCC)*, pp. 13-24.

Harlan, M. (2004). *Field Test of a Bridge Deck with Glass Fiber Reinforced Polymer Bars as the Top Mat of Reinforcement*, M.S. Thesis, Virginia Polytechnic Institute and State University, Blacksburg, VA, 2004.

Litherland, K.L., Oakley, D.R., Procter, B.A. (1981). The Use of Accelerated Aging Procedure to Predict the Long Term Strength of GRC Composites, *Cement and Concrete Research*, Vol. 11, pp. 455-466.

Micelli, F. Nanni, A., La Tegola, A. (2001). Effects of Conditioning Environments on GFRP Bars, *22ⁿᵈ SAMPE Europe International Conference,* CNIT Paris, pp. 1-13.

Phillips, K. (2004). *Performance of a Bridge Deck with Glass Fiber Reinforced Polymer Bars as the Top Mat of Reinforcement.* Unpublished master's thesis, Virginia Polytechnic Institute and State University, Blacksburg, VA.

Precast/Prestressed Concrete *Institute (1999). PCI Design Handbook,* Fifth Edition.

Zokaie, T., Osterkamp, T.A., and Imbsen, R.A. (1991). *Distribution of Wheel Loads on Highway Bridges.* NCHRP Report 12-26, Transportation Research Board, Washington, D.C.